

## PDF hosted at the Radboud Repository of the Radboud University Nijmegen

The following full text is a publisher's version.

For additional information about this publication click this link.

<http://hdl.handle.net/2066/19470>

Please be advised that this information was generated on 2017-12-05 and may be subject to change.



Torque Magnetometry Studies  
of Two-Dimensional Electron Systems



Torque Magnetometry Studies of Two-Dimensional Electron Systems

Maaïke Ruth Schaapman

Thesis, Katholieke Universiteit Nijmegen

Illustrated

With references - With summary in Dutch

Cover photo: Bert Beelen

ISBN 90-9018089-3

# Torque Magnetometry Studies of Two-Dimensional Electron Systems

een wetenschappelijke proeve op het gebied van de  
Natuurwetenschappen, Wiskunde en Informatica

Proefschrift

ter verkrijging van de graad van doctor  
aan de Katholieke Universiteit Nijmegen,  
op gezag van de Rector Magnificus Prof. dr. C.W.P.M. Blom,  
volgens besluit van het College van Decanen  
in het openbaar te verdedigen op  
dinsdag 6 juli 2004  
des namiddags om 3.30 uur precies

door

Maaïke Ruth Schaapman

geboren op 25 juni 1975  
te Delft

Promotor: Prof. dr. ir. J. C. Maan

Co-promotor: Dr. P. C. M. Christianen

Manuscriptcommissie: Prof. dr. A. D. Wieck  
(Ruhr-Universität Bochum, Germany)

Dr. D. Grundler  
(University of Hamburg, Germany)

Dr. U. Zeitler

# Voorwoord

Na een drukke tijd ben ik dan nu toe aan het schrijven van het laatste stukje proefschrift. Uit het raam van mijn kantoor in het nieuwe HFML zie ik de nieuwbouw van de rest van de faculteit en realiseer ik me hoeveel er in de afgelopen paar jaar veranderd is. De verhuizing met het lab en de creativiteit die nodig was om de vaten met helium het nieuwe gebouw in te krijgen voordat de bestrating en de tunnel klaar waren, zullen mij nog lang bij blijven.

Hoewel dit ‘mijn’ proefschrift is, was het werk waarover je in de komende hoofdstukken kunt lezen niet mogelijk geweest zonder de ondersteuning en input van een heleboel mensen, iedereen van het HFML en ook velen daarbuiten, die ik bij deze gelegenheid dan ook van harte wil bedanken.

In het bijzonder was er geen magnetometer geweest zonder de hulp van Jos Rook, Henk en Lijnis. Jos vertaalde mijn ideeën, krabbels en artistieke impressies in een bruikbaar ontwerp en een werkende insert. Henk wist voor al mijn electronica problemen een oplossing met een toepasselijke Henk-doos en hij kon altijd op korte termijn iets aanpassen als ik bedacht had dat ik toch net iets anders wilde. Lijnis zorgde voor veel van de extra onderdelen, onder andere de ‘zwarte doos’ voor de optica.

Voor de dagelijkse begeleiding wil ik drie mensen bedanken. Vanaf het moment dat ook ik besloot om op optica over te stappen, heeft Peter mij op weg geholpen en hij was daarna altijd een aanspreekpunt om te praten over praktische en inhoudelijke problemen. The many discussions I had with Andrey Geim at the start of my PhD-project have really helped me on my way, particularly his encouragement to throw away the old magnetometer and build this new one. Na zijn komst naar Nijmegen heeft ook Uli veel tijd in dit project gestoken. Ik ben blij dat mijn werk niet in de kast gezet wordt en wens jou en Iris veel succes de komende jaren.

Good research is not possible without good samples. I would like to thank Dirk Reuter, Dieter Schuh, and Maik Hauser for the 2DEG samples that have provided such nice results. I also would like to thank Werner Biberacher for the sample of  $\kappa$ -(BEDT-TTF)<sub>2</sub>Cu(NCS)<sub>2</sub>, a compound that produces really enormous de Haas-van Alphen oscillations.

Omdat 2DEG samples aan de achterkant meestal niet reflecterend zijn, is het nodig ze te poleisten. Jan Hermsen bedankt voor alle tijd en moeite die je hier in gestoken hebt.

Helaas besloot de 18.5 T supergeleider al snel na de start van mijn onderzoek langzaam maar zeker de geest te geven, wat gepaard ging met grote wolken helium. Jan van Benthum, bedankt voor de hulp in de moeizame onderhandelingen over de reparatie. Onze tocht naar Oxford zal mij nog lang bij blijven, vooral het hopelijk laatste zicht (van zee) op de rotsen van Dover. Toen er weer gewerkt kon worden, was er natuurlijk nog meer helium nodig en ik wil Frits en Ronald bedanken voor de volle vaten die ik ook op korte termijn en afwijkende tijden altijd nog kon krijgen.

Met mijn collega promovendi, Cecilia, Cécile, Eric, Fabio, Frans, Freddy, Giorgia, Hans, Igor, Kostya, Marius en Vadym, heb ik genoeg ergernissen, successen en grappige momenten gedeeld om een tweede boekje mee te vullen. Ik kon altijd bij Freddy en Eric terecht voor een praatje. Freddy, bedankt voor het babysitten tijdens de enige nacht van mijn promotie waarin ik gebruik maakte van de ‘grote’ installatie. Dankzij Cécile werd zelfs ik een trouwe bezoeker van het sportcentrum. For all my foreign colleagues: it was great fun to be a part of such an international group, thanks.

Adri, Harry, Hung, Jos P., Marijn, Stef O., Stef W. en Ramon bedankt voor de technische ondersteuning en de goede sfeer in het lab. Martha en Ine, bedankt voor alle administratieve hulp en natuurlijk de gezelligheid.

Naast het onderzoek is er natuurlijk ook ontspanning nodig. Met plezier denk ik terug aan alle gezellige weekendjes met mijn vriendinnen. Anne, Hester, Hester, Maartje, Maria en Marieke, bedankt! Dat er nog maar vele weekendjes mogen volgen en op naar de volgende promotie.

Last, but not least wil ik iedereen bedanken die voor mij zorgde toen ik ziek was, vooral mama, Gerwin en Sjoerd. Ik kan gelukkig altijd in Groesbeek terecht voor support en gezelligheid. Lieve Sjoerd, jij hebt een grote bijdrage geleverd aan dit boekje. Met liefde en begrip, maar ook praktisch en inhoudelijk met samples, helpen helium vullen, lezen en nog

veel meer.

**Bedankt!**

Maaike





# Contents

<b>Voorwoord</b>	<b>5</b>
<b>1 Introduction</b>	<b>13</b>
References . . . . .	16
<b>2 Two-dimensional systems of electrons</b>	<b>19</b>
2.1 Introduction . . . . .	19
2.2 The two-dimensional electron gas . . . . .	20
2.2.1 Realizing a 2DEG . . . . .	20
2.2.2 Energy-level structure in a 2DEG . . . . .	23
2.3 Magnetization . . . . .	27
2.3.1 Determining the magnetization of electrons . . . . .	27
2.3.2 The $1 \mu_{\text{B}}^*$ per electron saw-tooth . . . . .	29
2.3.3 Magnetization and the Fermi energy . . . . .	31
References . . . . .	32
<b>3 A multipurpose torsional magnetometer with optical angular detection</b>	<b>35</b>
3.1 Introduction . . . . .	36
3.2 The magnetometer . . . . .	37
3.2.1 Torsional magnetometry . . . . .	37
3.2.2 Optical angular detection . . . . .	38
3.2.3 Influence of the laser . . . . .	41
3.2.4 Feedback . . . . .	44
3.3 Application of the technique . . . . .	47
3.3.1 Magnetization of $\kappa$ -(BEDT-TTF) $_2$ Cu(NCS) $_2$ . . . . .	48
3.3.2 Magnetization of a 2D electron system . . . . .	49

3.4	Conclusion . . . . .	52
3.5	Acknowledgments . . . . .	52
	References . . . . .	52
<b>4</b>	<b>Magnetization of a two-dimensional electron gas</b>	<b>55</b>
4.1	Introduction . . . . .	55
4.2	Magnetization of the single layer, single subband 2DEG . .	57
	4.2.1 Landau-level transitions . . . . .	57
	4.2.2 Enhanced spin-splitting . . . . .	59
4.3	Conclusion . . . . .	60
	References . . . . .	60
<b>5</b>	<b>Magnetization of a two-dimensional electron gas with a second filled subband</b>	<b>63</b>
5.1	Introduction . . . . .	64
5.2	Experimental results . . . . .	65
5.3	Self-consistent field-dependent model . . . . .	66
5.4	Exchange-enhanced ground states . . . . .	70
5.5	Conclusion . . . . .	72
5.6	Acknowledgments . . . . .	72
	References . . . . .	72
<b>6</b>	<b>Magnetization of bilayer two-dimensional electron systems</b>	<b>75</b>
6.1	Introduction . . . . .	76
6.2	Experimental results . . . . .	78
	6.2.1 Magnetization of the 40 Å barrier bilayer 2DEG . .	78
6.3	The symmetric-anti-symmetric energy-splitting $\Delta$ SAS . . .	80
	6.3.1 Tilt-angle dependence of $\Delta$ SAS . . . . .	80
	6.3.2 Effect of $\Delta$ SAS on the magnetization . . . . .	82
	6.3.3 Size of the $\Delta$ SAS energy-splitting . . . . .	85
6.4	Reduced oscillations at Landau gaps . . . . .	89
	6.4.1 Magnetization at Landau-level transitions . . . . .	89
	6.4.2 In-plane magnetization . . . . .	91
	6.4.3 Filling factor dependence of the reduction . . . . .	92
6.5	Conclusion . . . . .	95
	References . . . . .	96

*Contents*

---

<b>Summary</b>	<b>97</b>
<b>Samenvatting</b>	<b>99</b>
<b>List of publications</b>	<b>101</b>
<b>Curriculum Vitae</b>	<b>103</b>

*Contents*

---

# Chapter 1

## Introduction

Since its discovery in 1897 by J.J. Thompson, the electron has initiated great advancements in both science and technology. In the early years of the 20<sup>th</sup> century the behavior of the electron has played a prominent role in the development of the now widely known and used theory of quantum mechanics. A major contribution to this theory was made by N. Bohr, who first suggested that the orbital angular momentum of electrons is quantized. In the 1930's, much work was done to improve the understanding of properties of the electrons responsible for current conduction in metals. Scientists, for example P. Drude and A. Sommerfeld, developed a model that treats these electrons as a gas with free movement in three directions (or dimensions). To simplify their task, amongst other approaches, theorists also reduced the three-dimensional electron gas to a two-dimensional electron gas (2DEG). While this two-dimensional electron gas is now one of the most widely experimentally studied physical systems, at that time this was considered to be highly unlikely, as we can read in R. Peierls opinion in 1933:

Wir wollen die Verhältnisse zunächst in einem noch einfacheren, aber physikalisch sinnlosen Fall diskutieren, ... Dazu betrachten wir einen zwei-dimensionalen Fall, ... [1]

One of the most important technological innovations to emerge from research into the properties of electrons is the transistor, which was invented in 1947 by J. Bardeen and W. Brittain. The transistor and the subsequently developed integrated circuit, invented in 1958 by J. Kilby,

have become an inseparable part of our daily lives in the electronic equipment that surrounds us. Both these inventions are also considered of such scientific importance that they were awarded the Nobel prize in physics [2] in 1956 and 2000 respectively.

Experimental investigations of the model of the 2DEG considered by Peierls, became possible as a direct result of the development of a new type of transistor: the silicon metal-oxide-semiconductor field-effect transistor (MOSFET). This is the first device that realizes the 2DEG. These investigations have led to many interesting discoveries. In 1980 Klaus von Klitzing discovered the quantum Hall effect [3] when studying the 2DEG in a MOSFET; he was awarded the Nobel prize for this in 1985. What he observed were very precisely quantized, equidistant plateaux at integer spacings in the Hall resistance of the 2DEG. This quantization is in fact universal and so precise that it is now used as an international standard to calibrate all other resistances by [4].

A few years later, in 1982, Daniel Tsui and Horst Störmer did similar experiments on a 2DEG in the better quality semiconducting material gallium-arsenide (now used in for example mobile phones and satellite receivers). They not only observed the plateaux found by von Klitzing at integer quantization, but they also found plateaux at odd-denominator fractional quantization [5]. Tsui and Störmer received the Nobel prize for this discovery of the fractional quantum Hall effect in 1998, together with Robert Laughlin who developed a partial theoretical understanding [6]. As we know now, in the fractional quantum Hall effect a plateau occurs when the 2D electrons form a new lowest energy state that is not determined by the properties of a single electron, but by the interactions between them. Both these famous discoveries have inspired many ingenious and innovative experimental and theoretical investigations that have resulted in a vast number of scientific publications. The number of publications in this quantum Hall effect field is still steadily rising and now amounts to 300 per year, i.e. one new publication daily.

The subject matter of this thesis, the magnetization of two-dimensional electron systems, roots in this field. It also roots in another field of condensed matter physics: Fermiology. Fermiology studies the fundamental properties of electrons in conducting materials through magnetization measurements. The technique was originally used to study electrons in metals, where it continues to be valuable. Nowadays it is usually employed

---

to study more exotic systems, such as for example highly anisotropic organic conducting materials. We shall see an example of this, the organic conductor bis(ethylenedithio)-tetrathiafulvalene, in chapter 3.

All materials with free electrons have in common that at low temperatures and in high magnetic fields, their magnetization becomes highly oscillatory. This behavior was first found by Landau in his calculations of the magnetization of a gas of free electrons in 1930 [7]. Although Landau himself dismissed this result as experimentally unobservable, in the same year the effect was first seen in bismuth by W.J. de Haas and P.M. van Alphen after whom the oscillations are now named.

The de Haas-van Alphen oscillations of electrons in the two-dimensional electron gas in a semiconductor that we will study in this thesis are very small. As a result highly sensitive magnetometers and high quality samples are needed. The first measurements were only possible in 1983 [8] and even then it was still necessary to use many parallel two-dimensional gases of electrons. The first measurements on a single 2DEG were done as recently as 1997 [9].

Magnetometry allows us to study one of the fundamental, thermodynamic ground state properties of electrons, which is not possible in the more common measurements of electrical conductivity. Therefore it is worthwhile to develop a magnetometry technique with enough sensitivity to detect the signal of a 2DEG. By using the technique on well chosen electron systems, we can study the single-particle properties of electrons and the effect of interactions between them. With these results we can try to shed some light on the question of what makes up the magnetic moment of electrons.

This thesis is divided into six chapters. After this general introduction, chapter 2 will introduce the 2DEG and its magnetization. Ways of realizing a 2DEG and the multi-component 2DEGs used in later chapters are explained along with some basic concepts, such as the energy-level structure. A simple model for the magnetization of a single-component 2DEG is also presented.

Chapter 3 will present the experimental setup: a sensitive, multipurpose torsional magnetometer with optical detection of the torque. The optical detection scheme and the feedback system of the magnetometer are characterized and the influence of the stray laser light on the sample



is measured and discussed. Sensitivity and versatility are demonstrated by measurements of the magnetization of the organic conductor  $\kappa$ -(BEDT-TTF)<sub>2</sub>Cu(NCS)<sub>2</sub> and of a multisubband two-dimensional electron gas.

Chapter 4 will investigate the magnetization of a single component 2DEG, and the expected, saw-tooth shaped de Haas-van Alphen oscillations with an amplitude of  $1 \mu_B^*$  per electron are observed. A finite step width indicates the presence of a background density of states, and, features observed at the lowest temperature suggest the spin-gap is enhanced by many-body interactions.

Chapter 5 will show the magnetization of the 2DEG with a second filled subband in a heterojunction (the dual-subband 2DEG). In contrast to the single subband 2DEG described in the previous chapter, non- $1/B$ -periodic, triangularly shaped oscillations of the magnetization with an amplitude significantly less than  $1 \mu_B^*$  per electron are observed. All three effects are explained by a field dependent self-consistent model of the energy-level structure. At 1 K additional, not previously observed minima in the magnetization are present at Landau-level crossings.

Chapter 6 will discuss the magnetization of the bilayer 2DEG. At filling factors where a symmetric-anti-symmetric transition occurs, steps in magnetization are observed, even though this transition is purely electronic in nature. Surprisingly, the apparent size of the magnetization steps associated to the Landau-level transitions is found to be significantly reduced compared to the value typical for a single subband two-dimensional electron system. This large reduction is speculated to be due to the presence of an in-plane component of the magnetization.

## References

- [1] R. Peierls, Z. Phys. **81**, 186 (1933).
- [2] [www.nobel.se/physics](http://www.nobel.se/physics).
- [3] K. von Klitzing, G. Dorda, and M. Pepper, Phys. Rev. Lett. **45**, 494 (1980).
- [4] [www.ptb.de/en/org/2/Inhalte/qhe/E-quantenhalleffekt.htm](http://www.ptb.de/en/org/2/Inhalte/qhe/E-quantenhalleffekt.htm).

- [5] D. C. Tsui, H. L. Störmer, and A. C. Gossard, Phys. Rev. Lett. **48**, 1559 (1982).
- [6] R. B. Laughlin, Phys. Rev. Lett. **50**, 1395 (1983).
- [7] L. Landau, Z. Phys. **64**, 629 (1930).
- [8] H. L. Störmer, T. Haavasoja, V. Narayanamurti, A. C. Gossard, and W. Wiegmann, J. Vac. Sci. Technol. B **1**, 423 (1983).
- [9] S. A. J. Wieggers, M. Specht, L. P. Lévy, M. Y. Simmons, D. A. Ritchie, A. Cavanna, B. Etienne, G. Martinez, and P. Wyder, Phys. Rev. Lett. **79**, 3238 (1997).



# Chapter 2

## Two-dimensional systems of electrons

### Abstract

The two-dimensional electron gas (2DEG) and its magnetization are introduced. Typical realizations of 2DEGs are explained along with possibilities to add an extra degree of freedom, resulting in a multi-component system. We show that the energy-level structure, which is intimately connected with the magnetization, is a combination of the quantized levels of the confining potential, the Landau-levels and the spin-splitting. Using this energy-level structure, we present two ways of calculating the magnetization: i. by taking the derivative of the free energy, and ii. via a Maxwell relation. A simple approximation for a single component 2DEG shows the magnetization to be a  $1/B$ -periodic saw-tooth with an amplitude of  $1 \mu_B^*$  per electron.

### 2.1 Introduction

The two-dimensional electron gas (2DEG), a system where electrons are confined by a potential well in one direction, but free to move in the two perpendicular ones, is an excellent model system for studying the properties of electrons. The reduction from three to two dimensions generally

simplifies the physics, and also changes the strength of the interactions. As a result the contributions of single particles to the electronic properties as well as those caused by many-body effects [1, 2] become much clearer. Here the 2DEG with some of its interesting properties and experimental possibilities is introduced. The study of the magnetization, or more precisely the de Haas-van Alphen oscillations of 2DEGs forms the backbone of this thesis. The importance of this property, which is particularly interesting since it gives direct access to the thermodynamics of the system, is explained.

## 2.2 The two-dimensional electron gas

### 2.2.1 Realizing a 2DEG

The 2DEGs used for the work in this thesis are realized in semiconductor structures made from GaAs and  $\text{Al}_x\text{Ga}_{1-x}\text{As}$ , with an aluminum content of typically  $x = 0.3$ . An important advantage of these two materials is that, while they have a different gap between the valence and the conduction band, the lattice constants of the two crystals are nearly the same [3]. Consequently both materials can be grown on top of each other incorporating almost no strain, resulting in smooth interfaces and very few dislocations. The structures are grown using molecular beam epitaxy (MBE) [4]. In this technique high purity GaAs and AlGaAs are grown, layer by layer, onto a heated GaAs substrate in ultra high vacuum. The resulting crystal has a minimal number of imperfections. This high quality crystal and the smooth interface result in a 2DEG where electrons have a mean free path exceeding several micrometers; in other words, an electron can travel tens of thousands of atomic spacings before being scattered. The electrons can therefore essentially be treated as a ‘free’ gas in two dimensions as there is very little interaction with (impurities in) the lattice. There are two typical ways to realize a 2DEG: a heterojunction and a quantum well.

In a heterojunction AlGaAs doped with Si is grown onto undoped GaAs. In equilibrium the chemical potential of the resulting crystal has to be continuous across the interface, causing the doping electrons to accumulate at this interface. The charge separation causes an electric field, leading the conduction band to bend downwards. An approximately triangular potential well is formed that confines the electrons in the growth

direction  $z$ , but leaves them free to move in the perpendicular  $x, y$ -plane (Figure 2.1). The number of electrons in the 2DEG can be easily adjusted via higher (or lower) doping by substituting more (or less) of the Ga atoms in the AlGaAs with Si. This replacement of Ga in the AlGaAs is called remote doping [5] and has the additional advantage that the positively charged Si ions are spatially separate from the electrons in the 2DEG, thus minimizing their scattering probability with the doping atoms, leading to a high quality 2DEG.

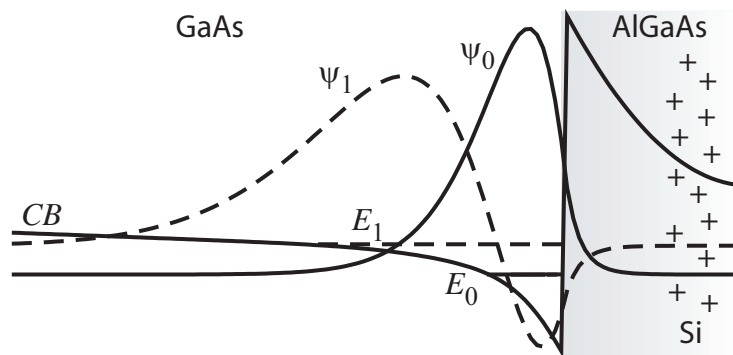


Figure 2.1: Schematic representation of a 2DEG in a GaAs/AlGaAs heterojunction (+ indicates the presence of remote doping with Si); bending of the conduction band  $CB$  in GaAs can be seen at the interface. The level  $E_0$  and wavefunction  $\psi_0$  of the lowest electronic energy are indicated by a solid, that of first excited level,  $E_1$  and  $\psi_1$ , by a dashed line.

The heterojunction is illustrated in figure 2.1, which shows the confining potential in the GaAs and the AlGaAs, where the presence of remote doping is also indicated (+). The lowest energy level  $E_0$  and its wavefunction  $\psi_0$  are indicated with a solid line, the second energy level  $E_1$  and its wavefunction  $\psi_1$  by the dashed lines. Usually, the electron density has a value such that only the lowest electronic energy level of the triangular well is occupied. Such a single component 2DEG is studied in chapter 4. A two-component 2DEG in a heterojunction can be formed by increasing the electron density to fill a second electronic subband. This dual-subband 2DEG has some interesting properties related to the nature of the confinement of the 2DEG and is presented in chapter 5.

A second way to realize a 2DEG is by forming a quantum well, where a thin layer of GaAs is sandwiched in between two (much thicker) layers of AlGaAs. Because the conduction band in GaAs is lower than that of AlGaAs, a square quantum well is now formed by the crystal potential. Electrons are confined in this well and again movement is only possible in a plane perpendicular to the well. Also in this structure remote Si-doping is used to control the electron density in the 2DEG. The quantum well is illustrated in figure 2.2.

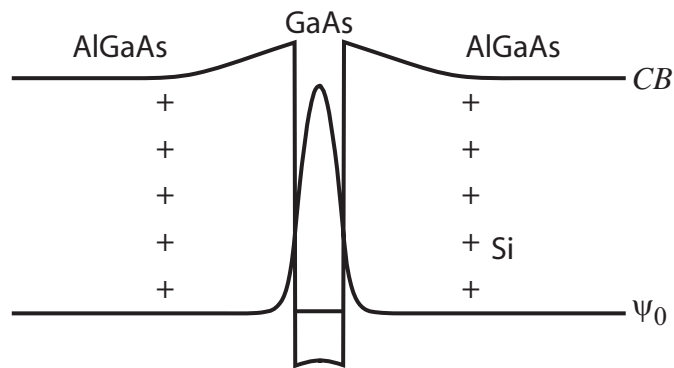


Figure 2.2: Schematic representation of a 2DEG in a quantum well. The confining potential is formed by the conduction band of the crystal. The shape of the electron wavefunction  $\psi_0$  shows the confinement in the well.

This second approach of making a 2DEG allows different ways of making multi-component systems. A double quantum well, the system we will use, is formed by adding a thin AlGaAs layer followed by a second GaAs layer to the first quantum well. The fact that the confining potential is determined by the deliberately grown structure of this two-component system, means it can be easily manipulated. The coupling between the components (tunnelling as well as Coulomb interaction) can be varied by choosing different barrier widths and heights. It also means the system has the added interest of having an extra degree of freedom, making it neither purely 2D nor really 3D. In chapter 6 we study the magnetization of 2DEGs in double quantum wells that have a barrier thin enough for electrons to tunnel between the wells. This system is generally referred to as a bilayer 2DEG.

### 2.2.2 Energy-level structure in a 2DEG

As we will see in the next paragraph (and throughout this thesis), the key to understanding the magnetization of a 2D electron gas is the knowledge of its energy-level structure and how it changes when a magnetic field is applied.

In zero magnetic field the 2D gas of electrons has a density of states (DOS,  $D(E)$ ) given by  $D(E) = m^*/\pi\hbar^2$ , a constant. In this expression we have made use of the effective mass approximation. This approximation, which works well for GaAs, describes the electrons as free electrons with an effective mass  $m^*$  that accounts for the influence of the crystal; in GaAs  $m^* = 0.0665m$  [6], with  $m$  the mass of a free electron in vacuum. Electrons continuously fill this constant DOS up to the Fermi energy  $E_F$ .

When a magnetic field  $B$  is applied perpendicular to the 2DEG:  $\mathbf{B} = B\mathbf{e}_z$ , the Lorentz force restricts the motion of the electrons and consequently the DOS changes drastically. When the Landau-gauge is used for the vector potential ( $\mathbf{A} = (0, Bx, 0)$ ), the Hamiltonian is given by

$$\mathcal{H} = \frac{1}{2m^*} \left[ p_x^2 + (p_y^2 + eBx)^2 \right] \quad (2.1)$$

with  $p_x, p_y$  and  $x$  the operators for momentum and position. The solution of this equation is a set of quantized, discrete energy-levels: Landau levels with energies  $E_r = (r + \frac{1}{2})\hbar\omega_c$  with  $r$  an integer, and  $\omega_c = eB/m^*$  the cyclotron frequency. The DOS now consists of sharp peaks with a spacing of  $\hbar\omega_c$  (illustrated in Figure 2.3), each having a degeneracy of  $2eB/h$ . The factor 2 accounts for spin-splitting (discussed in the next paragraph), if this is taken into account the degeneracy of each level is  $eB/h$ . The fraction  $\nu = hn/eB$ , with  $n$  the density of electrons in the 2DEG, gives the number of filled, spin-split Landau levels and is therefore commonly known as the “filling factor”. Although in an ideal system these peaks in the DOS are delta-functions, in reality they are broadened by disorder in the sample. This broadening is commonly described by a Gaussian distribution with a width  $\Gamma$  proportional to the square root of the magnetic field ( $\Gamma \sim \sqrt{B}$ ) [7–9], although strictly speaking this is only correct for short range scatterers [10–13], which might not be completely the case for 2D systems in GaAs.

Additionally to quantized circular motion (orbital angular momentum) electrons have spin 1/2. A free spin in a magnetic field contributes an



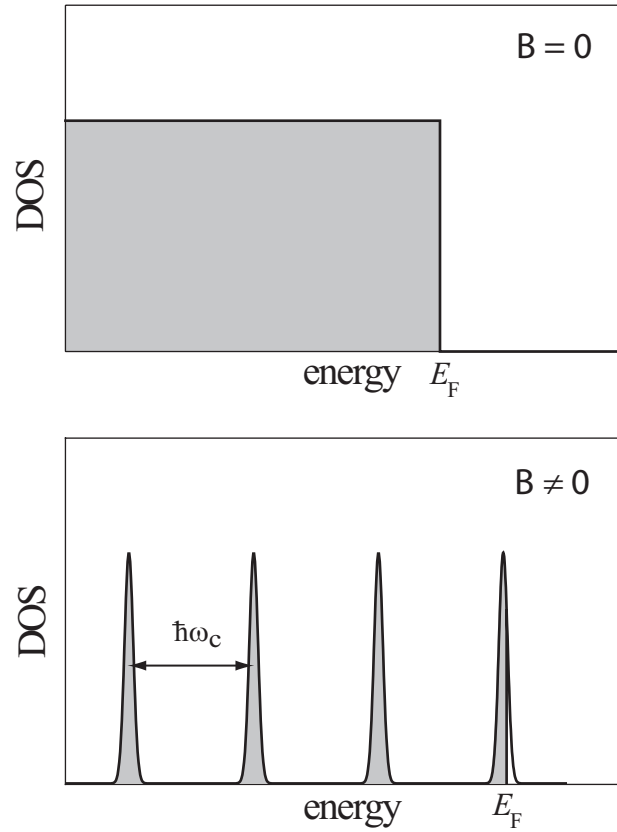


Figure 2.3: Density of states of the 2DEG. In 0 T the DOS is constant, but when a magnetic field is applied, it splits into discrete levels, here shown with Gaussian broadening.

energy of  $g_0\mu_B B S_z$ , where  $g_0$  is the gyromagnetic ratio,  $\mu_B = e\hbar/2m$  the Bohr magneton, and  $S_z$  the component of the spin along the magnetic field axis. The 2DEG electrons in GaAs can be described as free electrons with an effective  $g$ -factor of -0.44. Therefore each Landau-level is split into two levels by  $\pm\frac{1}{2}g\mu_B B$ , giving an extra energy gap of  $25 \mu\text{eV}/\text{T} \times B$ : i.e. two orders of magnitude smaller than the Landau-level splitting, which is  $1.7 \text{ meV}/\text{T} \times B$ .

Figure 2.4 shows a typical scheme of 2DEG energy levels as a function of magnetic field. The Fermi energy represents a 2DEG with an electron

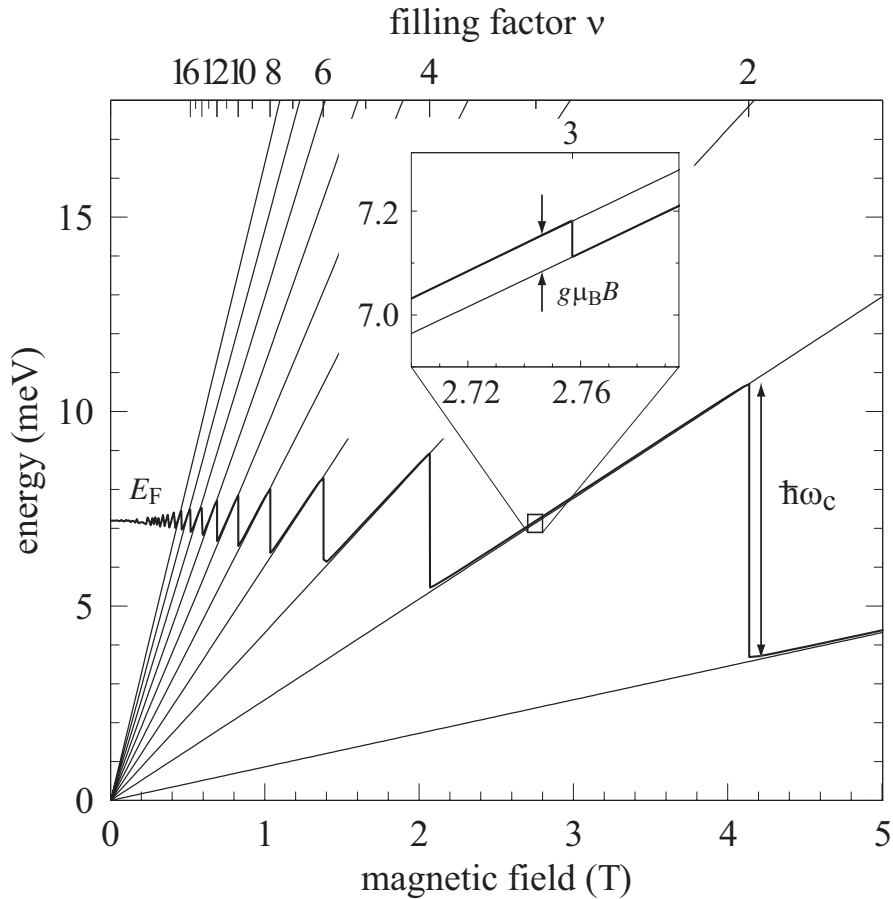


Figure 2.4: Energy level scheme of a 2DEG with  $n = 2.0 \cdot 10^{11} \text{ cm}^{-2}$ . The Landau level fan (thin lines) can clearly be seen, the Fermi energy oscillates as magnetic field is increased. Inset shows an enlargement of the area in the small square: the spin splitting only becomes visible on this scale.

density of  $n = 2 \cdot 10^{11} \text{ cm}^{-2}$ .  $E_F$  can be clearly seen to oscillate, jumping to a lower energy level when the highest energy (Landau) level is depopulated with increasing magnetic field (at even  $\nu$ ). Because the size of the spin-gap is too small to be visible compared to the Landau-gaps, it is enlarged in the inset for  $\nu = 3$ .

In the  $z$ -direction the 2DEG is confined in a potential with its own

quantized energy levels  $E_n$ , or electronic subbands, that depend on the shape of the well. The electrons contribute to the confining potential depending on their spatial distribution. This distribution can be calculated using the Poisson equation and is determined by the shape of the wavefunction, which in turn is connected with the energy levels. In other words: the Poisson and Schrödinger equations have to be solved self-consistently.

$$\begin{cases} \nabla^2 \Phi(z) = -\frac{\rho(z)}{\epsilon_0 \epsilon_r} \\ \left[ -\frac{\hbar^2}{2m^*} \nabla^2 + V(z) \right] \Psi(z) = E \Psi(z) \end{cases} \quad (2.2)$$

Here  $\Phi(z)$  is the electrostatic potential which determines the band bending,  $\rho(z)$  is the distribution of electrons resulting from the wavefunction  $\Psi(z)$ ,  $E$  the energy, and  $V(z)$  the confining potential.

When more than one electronic subband is occupied, the occupancy of the subbands becomes dependent on the magnetic field, because of the field dependence of the density of states. The energy levels  $E_{nr}(B)$  in the 2DEG are therefore expressed by:

$$E_{nr}(B) = E_n(B) + \left( r + \frac{1}{2} \right) \hbar \omega_c \pm \frac{1}{2} g \mu_B B \quad (2.3)$$

The magnetic field dependence of  $E_n$  is particularly strong for the heterojunction, where  $V(z)$  depends very strongly on  $\Psi(z)$  (note the very different extents of the two wavefunctions in Fig. 2.1).

Further details on the energy-level structure of a dual-subband 2DEG can be found in chapter 5, where a home-built Fortran program is used to numerically calculate the energy levels and Fermi energy of this system as a function of magnetic field. In quantum wells the GaAs/AlGaAs structure dictates the major part of the confining potential and consequently the magnetic field has only a marginal effect on the electronic subband energies. In this case Eq. (2.2) can be solved at zero field and in a magnetic field a fan of Landau-levels is superimposed onto this band structure.

The 2DEGs in a single quantum well and in a heterojunction with one occupied electronic subband are very similar, both showing the behavior depicted in Fig. 2.4. The energy-level structure of a bilayer is different since the two, coupled, single quantum wells form combined symmetric and anti-symmetric wavefunctions in each of the electronic subbands. As

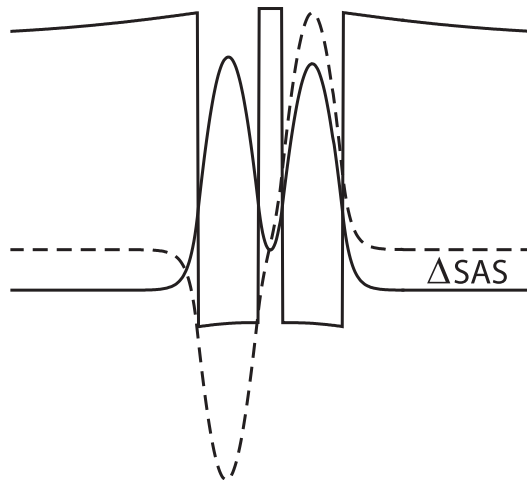


Figure 2.5: Symmetric (solid line) and anti-symmetric (dashed line) wavefunctions in a bilayer 2DEG. Their energy-levels are split by an extra symmetric-anti-symmetric energy splitting ( $\Delta$ SAS).

the anti-symmetric state is somewhat higher in energy, all original energy-levels are split into two by the symmetric-anti-symmetric energy splitting ( $\Delta$ SAS), illustrated in Figure 2.5. Instead of having the single Landau-level fan illustrated in Figure 2.4, the bilayer has two of these fans shifted in energy by the  $\Delta$ SAS. This effect and its consequences for the magnetization of the 2DEG are the subject of study in chapter 6.

## 2.3 Magnetization

### 2.3.1 Determining the magnetization of electrons

The first estimate of the magnetization of electrons was made by Landau as early as 1930 [14]. As pointed out by Peierls [15], this is equivalent to semi-classically summing the contributions of the electrons in their cyclotron orbits, as sketched for two dimensions in the left hand side of Figure 2.6. However, if we think of electrons in a magnetic field as little, quantized, circular currents in this way and consider the practical case of a finite size sample, we find that all the currents that are “cut off” at the edge form

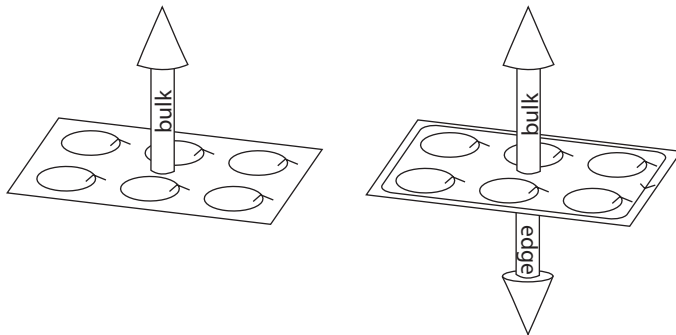


Figure 2.6: Proposed magnetic moment of the 2DEG. Left: it is the sum of orbital angular moments of the electrons in the Landau levels. Right: magnetic moment from the current resulting from the orbits cut off by the sample edge precisely compensates that of the bulk.

a total edge current with a magnetic moment that precisely compensates that of the bulk (illustrated in the right hand side of Figure 2.6). This reasoning would imply that the magnetization of a 2DEG must be zero at all times.

The approach of summing electron orbits was therefore immediately under debate. An extensive consideration of the problem was made by Peierls [15], who is the first to calculate the magnetic moment of a gas of free electrons through thermodynamics: by taking the derivative of the free energy with respect to the magnetic field. This approach is now universally used. In his work Peierls finds for a free gas of electrons a finite, oscillatory magnetic moment.

Indeed experiment has unambiguously proven that 2D electron systems do exhibit de Haas-van Alphen oscillations (the subject of this thesis). However, the importance of the edge is still under debate, in particular the contribution of equilibrium currents in quantum mechanical edge states is still unclear [16–18]. The magnetization of the 2DEG often shows a large feature at integer and fractional filling factors, the size and shape of which depend on the sweep-rate and direction of the magnetic field. This so called non-equilibrium “Eddy current” is also still studied in this context [19, 20].

### 2.3.2 The $1 \mu_B^*$ per electron saw-tooth

As the first measurements of the magnetization of a system of electrons confined in two dimensions were being performed in 1983 [21], the size and shape of this magnetization had already been under consideration by Shoenberg in what is now a standard work in 3D Fermiology: “Magnetic oscillations in metals” [22]. The magnetization is calculated for a fixed number of electrons  $N$  as a ‘digression’ from the usual assumption of a fixed chemical potential. Although the author indicates it is not straight forward that this calculation is indeed applicable to real 2DEG structures, experiments have shown it to be correct in oscillation period and phase [9, 23], and, with improving quality of samples and experimental data, a reasonable estimate of the shape [24].

In order to derive an expression for the magnetization  $M$ , several additional assumptions are made. First, we calculate  $M$  at 0 K, which can most easily be done by using the internal energy  $E$  instead of the free energy  $F$ . This leads to the following expressions for magnetization and Fermi energy.

$$M = -\left. \frac{\partial E}{\partial B} \right|_N \quad E_F = -\left. \frac{\partial E}{\partial N} \right|_B \quad (2.4)$$

In a magnetic field  $E$  consists of a series of energy levels  $E_r$  (Landau levels, spin splitting is ignored), assumed to be delta-functions. We fix  $E_F$  in the highest,  $p^{\text{th}}$ , partially occupied level.

$$E = O \sum_{r=0}^{p-1} E_r + (N - Op) E_p \quad (2.5)$$

In this expression  $O$  is the occupancy of each level: the lower Landau-levels are all fully occupied, and the top level contains the remaining electrons. The occupancy is simply the degeneracy of each energy level times the surface area  $A$  of the 2DEG:  $O = 2eB/h \times A$ , where the factor 2 accounts for the spin. To be able to take the partial derivative to  $B$ , the sum in Eq. (2.5) needs to be evaluated and to do this it is more convenient to introduce a continuous variable

$$\nu = 2\frac{N}{O} \quad \text{and} \quad E_F(\nu) \equiv E_F(0) \quad (2.6)$$

$\nu$  can be easily identified as the filling factor well known from the quantum Hall effect [1]. The evaluation of Equation (2.5) (extensive details can be

found in reference [22]) leads to an expression in several parts. As we want to know the shape of the de Haas-van Alphen oscillations of the 2DEG, we are only interested in the oscillatory part of  $E$ , given by

$$E_{osc} = -\frac{\mu_B^* B N}{\nu/2} \left[ \left( \frac{\nu}{2} - p \right)^2 - \left( \frac{\nu}{2} - p \right) + \frac{1}{6} \right] \quad (2.7)$$

By using Equation (2.4), it immediately follows that

$$M = -2\mu_B^* N \left[ \frac{\nu}{2} - \left( p + \frac{1}{2} \right) \right] \quad (2.8)$$

This expression for  $M$  is illustrated in Figure 2.7. It is a saw-tooth with an amplitude of  $1 \mu_B^*$  per electron, that oscillates with a period of  $2\nu$  (spin-splitting is neglected). It has sharp transitions at even  $\nu$ , where the highest occupied Landau level  $E_p$  is precisely depleted and the Fermi energy jumps to the level below it as  $\nu$  decreases.

In order to describe the finer details of the shape of the de Haas-van Alphen oscillations in a 2DEG, the use of a series of delta-functions for the energy levels and the assumption of zero temperature are too unrealistic. By using Fermi-Dirac statistics and assuming a fixed number of particles in the 2DEG, the magnetization can be calculated through thermodynamics [25] using the following set of equations:

$$M = -\left. \frac{\partial F}{\partial B} \right|_{N,T} \quad (2.9)$$

$$F = \mu N - kTA \int D(E) \ln \left[ 1 + \exp \left( \frac{\mu - E}{kT} \right) \right] dE \quad (2.10)$$

where  $\mu$  represents the chemical potential.

Although being much more realistic, Equations (2.9) and (2.10) have the disadvantage compared to Equation (2.8) of having to be solved numerically. Fortunately this is only a small price to pay, as the model has the great advantage of providing a tool to directly investigate the shape of the density of states through magnetometry [18, 26]. We will see an example of this in chapter 4.

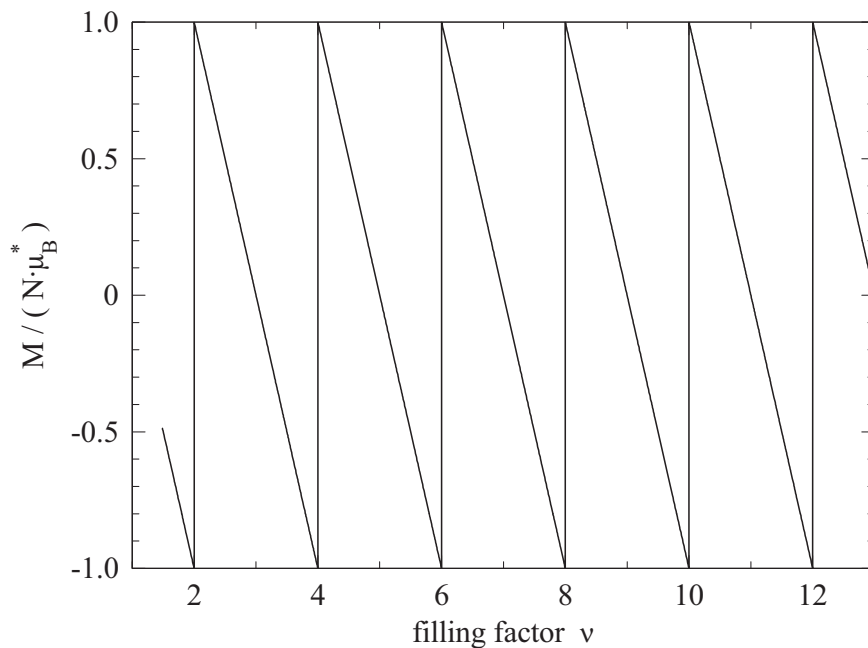


Figure 2.7: Magnetization of a single 2DEG, calculated using Eq. (2.8), the analytical model by Shoenberg [22]. Oscillations are saw-tooth shaped with an amplitude of  $1 \mu_B^*$  per electron. The sharp steps occur where  $E_F$  jumps from one Landau-level to the one below it.

### 2.3.3 Magnetization and the Fermi energy

Another way of determining the magnetization is by taking a second derivative and making use of the Maxwell equation that relates  $M$  to the chemical potential  $\mu$  of the 2DEG.

$$\left(\frac{\partial M}{\partial \mu}\right)_B = \left(\frac{\partial N}{\partial B}\right)_\mu \quad (2.11)$$

Note that in this (generally valid) equation  $N$  can vary with  $B$ . As we have seen, the peaks in the density of states of a 2DEG are proportional to the magnetic field and this reduces Eq. (2.11) to a simple proportionality between the changes in magnetization and the changes in the chemical potential. Although strictly speaking the Fermi energy is only equal to the



chemical potential at 0 K, at our experimental temperatures and electron densities the difference is negligible and we find that changes in the magnetization can be directly determined from changes in the Fermi energy.

$$\Delta M = \frac{N}{B} \Delta E_F \quad (2.12)$$

Here  $N$  again represents the constant number of electrons.

Reconsidering Figure 2.4, the magnetization that follows from Equation (2.12) is, as expected, a  $1/B$ -periodic sawtooth with an amplitude of  $1 \mu_B^*$  per electron at the steps at even  $\nu$ , well approximated by the analytical model shown in Figure 2.7.

On the one hand the proportionality given by Eq. (2.12) provides a way to describe the more complex multi-component 2DEGs. This description is used for the dual-subband 2DEG in chapter 5, where the Fermi energy is calculated along with the energy level structure by a built-in function of the same Fortran program that solves Equations (2.2).

On the other hand, from a more fundamental point of view, the proportionality also raises some interesting questions about the microscopic origin of the magnetization. Being a thermodynamic equation, (2.12) gives no information about changing quantum mechanical properties of the electrons. It simply states that *any* change in the Fermi energy, irrespective of what brings it about, will have a corresponding change in the size of the magnetic moment of the 2DEG. Therefore even a transition between purely electronic energy levels that does not involve a change in the properties which we normally associate with magnetism (orbital angular momentum or Landau level index and spin), must change the magnetization of the 2DEG. In a bilayer 2DEG precisely such a transition occurs: the symmetric-anti-symmetric transition (Fig. 2.5). The question of whether Eq. (2.12) holds in reality is part of the subject of chapter 6, which studies bilayer 2DEGs.

## References

- [1] T. Chakraborty and P. Pietiläinen, in *The Quantum Hall Effects*, Vol. 85 of *Solid State Sciences*, edited by M. Cardona, P. Fulde, K. von Klitzing, and H.-J. Queisser (Springer, Heidelberg, 1995).

- 
- [2] S. Das Sarma and A. Pinczuk, *Perspectives in Quantum Hall Effects* (Wiley, New York, 1997).
- [3] S. Adachi, J. Appl. Phys. **58**, R1 (1985).
- [4] P. Y. Yu and M. Cardona, *Fundamentals of Semiconductors, Physics and Materials Properties*, 3rd ed. (Springer, 2001).
- [5] H. L. Stormer, R. Dingle, A. C. Gossard, and W. Wiegmann, Inst. Conf. Ser. London **43**, 557 (1978).
- [6] I. Vurgaftman, J. R. Meyer, and L. R. Ram-Mohan, J. Appl. Phys. **89**, 5815 (2001).
- [7] V. Mosser, D. Weiss, K. v. Klitzing, K. Ploog, and G. Weimann, Solid State Commun. **58**, 5 (1986).
- [8] E. Gornik, R. Lassning, G. Strasser, H. L. Störmer, and W. Wiegmann, Phys. Rev. Lett. **54**, 1820 (1985).
- [9] J. P. Eisenstein, H. L. Stormer, V. Narayanamurti, A. Y. Cho, A. Gossard, and C. W. Tu, Phys. Rev. Lett. **55**, 875 (1985).
- [10] T. Ando, and Y. Uemura, J. Phys. Soc. Jpn. **36**, 959 (1974); T. Ando, J. Phys. Soc. Jpn. **37**, 622 (1974).
- [11] R. R. Gerhardts, Z.Phys. B **21**, 275 (1974); **21**, 285 (1974); Surf. Sci. **58**, 234 (1976)
- [12] H. Aoki, and T. Ando, Solid State Commun. **38**, 1079 (1981).
- [13] V. Gudmundsson, and R. R. Gerhardts, Phys. Rev. B **35**, 8005 (1987).
- [14] L. Landau, Z. Phys. **64**, 629 (1930).
- [15] R. Peierls, Z. Phys. **80**, 763 (1933); 186 (1933).
- [16] M. R. Geller, and G. Vignale, Phys. Rev. B **50**, 11714 (1994); **52**, 14137 (1995).
- [17] L. Bremme, T. Ihn, and K. Ensslin, Phys. Rev. B **59**, 7305 (1999).

- [18] M. P. Schwarz, M. A. Wilde, S. Groth, D. Grundler, C. Heyn, and D. Heitmann, *Phys. Rev. B* **65**, 245315 (2002).
- [19] J. P. Watts, A. Usher, A. J. Matthews, M. Zhu, M. Elliott, W. G. Herrenden-Harker, P. R. Morris, M. Y. Simmons, and D. A. Ritchie, *Phys. Rev. Lett.* **81**, 4220 (1998).
- [20] A. J. Matthews, J. P. Watts, M. Zhu, A. Usher, M. Elliott, W. G. Herrenden-Harker, P. R. Morris, M. Y. Simmons, and D. A. Ritchie, *Phys. E* **6**, 140 (2000).
- [21] H. L. Störmer, T. Haavasoja, V. Narayanamurti, A. C. Gossard, and W. Wiegmann, *J. Vac. Sci. Technol. B* **1**, 423 (1983).
- [22] D. Shoenberg, *Magnetic oscillations in metals, Cambridge monographs on physics* (Cambridge University Press, Cambridge, 1984).
- [23] J. P. Eisenstein, H. L. Störmer, V. Narayanamurti, and A. C. Gossard, *Superlattice Microstruct.* **1**, 11 (1985).
- [24] S. A. J. Wieggers, M. Specht, L. P. Lévy, M. Y. Simmons, D. A. Ritchie, A. Cavanna, B. Etienne, G. Martinez, and P. Wyder, *Phys. Rev. Lett.* **79**, 3238 (1997).
- [25] C. J. Adkins, *Equilibrium Thermodynamics*, 3rd ed. (Cambridge University Press, Cambridge, 1983).
- [26] A. Potts, T. Shepherd, W. G. Herrenden-Harker, M. Elliott, C. L. Jones, A. Usher, D. A. Ritchie, E. H. Linfield, and M. Grimshaw, *J. Phys.: Condens. Matter* **8**, 5189 (1996).

## Chapter 3

# A multipurpose torsional magnetometer with optical angular detection

### Abstract

We have developed a sensitive, multipurpose torsional magnetometer with optical detection of the torque. The use of a feedback system with a current coil mounted with the sample allows direct, quantitative determination of the magnetization with a sensitivity of  $10^{-12}$  J/T in a Bitter-magnet and  $2 \cdot 10^{-13}$  J/T at 15 T in a superconducting magnet. The system can be used over a wide range of temperatures and up to high magnetic fields. To demonstrate the sensitivity and versatility of our magnetometer, we present magnetization measurements of a 0.13 mg crystal of the organic conductor  $\kappa$ -(BEDT-TTF)<sub>2</sub>Cu(NCS)<sub>2</sub> and of a multisubband two-dimensional electron gas.

---

Part of this work has been published in:  
M. R. Schaapman, P. C. M. Christianen, J. C. Maan, D. Reuter, and A. D. Wieck, Appl. Phys. Lett. **81**, 1041 (2002).

## 3.1 Introduction

Magnetometry is a tool that is widely used in condensed matter physics to study the properties of a great variety of physical systems. Because measurements are often done at high magnetic fields in which the amount of available space is limited, signals are typically small. To detect these small magnetization signals a sensitive magnetometer is needed. Torsional magnetometers are very suitable for this purpose, since they have a high sensitivity and can be used up to very high magnetic fields. In order to study the magnetization of a variety of systems with this technique, we have developed a versatile and highly sensitive torsional magnetometer with optical angular detection that is capable of supporting large samples and can be operated from room temperature down to 1 K.

For an optimal performance, many different types of torsional magnetometers have been designed. One of the most used is the cantilever [1]. Although a high sensitivity can be achieved, designs are often highly specialized and can only be used for one sample or type of sample. A sensitive cantilever has the added disadvantage of only being able to support very light and therefore small samples. In this way much of the gain in sensitivity is lost, since the signal-to-noise ratio is not improved. Our design is a wire-based torque magnetometer. The absolute sensitivity that can be reached in such a design is somewhat less, but the signal to noise ratio that can be reached is higher as it has the possibility to mount large samples.

Many cantilevers [1–3] and other wire torque magnetometers [4–7] use electronic detection methods, such as capacitive detection. Capacitive detection requires a large electric field, which, because of the limited amount of space, is near the sample. To avoid this, we have developed an optical detection system that also ensures no unwanted electronic signals, such as capacitive coupling, can influence the measurements. In addition our optical detection is independent of properties of the experimental environment, such as the dielectric constant, which allows the device to be used over a wide range of temperatures with the same sensitivity. The magnetometer can be operated in a superconducting magnet as well as in a Bitter-magnet. The combination of a wide range of temperatures (including room temperature) with operation in a Bitter-magnet opens the possibility for measurements on systems from chemistry and biology as well.

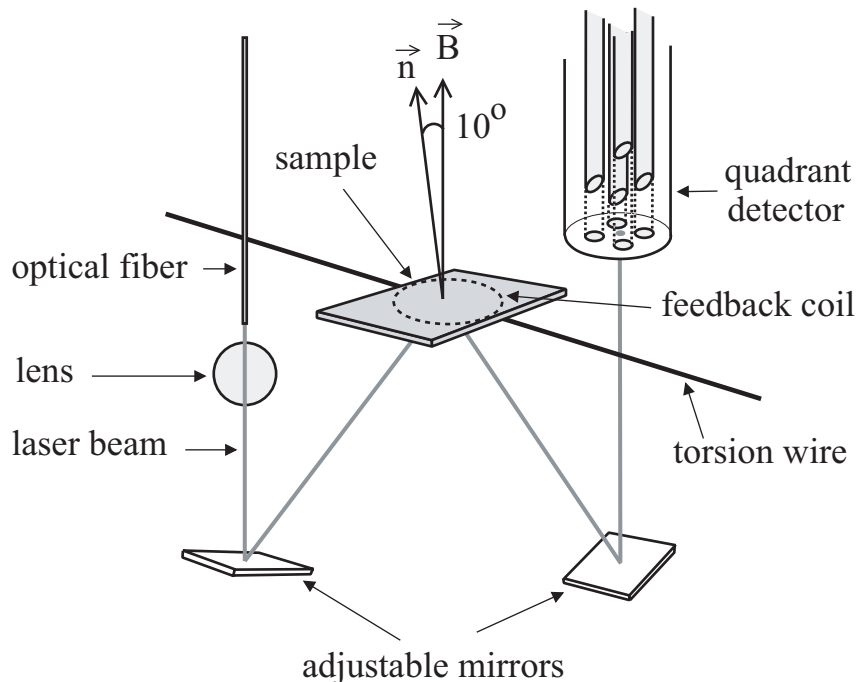


Figure 3.1: Schematic representation of the magnetometer. The laser beam is reflected from the sample onto the detector, which detects a displacement when the sample rotates. The dashed circle on the sample indicates the position of the feedback loop underneath the sample.

## 3.2 The magnetometer

### 3.2.1 Torsional magnetometry

The principle on which our magnetometer (schematically shown in Fig. 3.1) is based is similar to that of other torsional magnetometers: torque is translated into a displacement, which is detected. This detection can be done in several ways, for example capacitively [4, 8], or optically [9] as we do here.

The torque  $\Gamma$  experienced by a magnetic moment  $\mathbf{M}$  in a magnetic field  $\mathbf{B}$  and at a distance  $\mathbf{r}$  from the rotation axis is given by

$$\Gamma = \mathbf{M} \times \mathbf{B} + \mathbf{r} \times (\mathbf{M} \cdot \nabla) \mathbf{B} \quad (3.1)$$

When the sample is mounted on the rotation axis and placed in a homogeneous magnetic field, the second term in Equation (3.1) is zero. A torque will only be detected if the sample is anisotropically magnetized at a small angle with the magnetic field. The (orbital) magnetization of two-dimensional electron systems, the subject of this thesis, is anisotropic and usually perpendicular to the sample. A compromise between maximum torque and minimum in-plane magnetic field results in the angle of  $10^\circ$  depicted in Fig. 3.1. When the sample is mounted away from the rotation axis and a field gradient is applied, the magnetometer is also sensitive to a magnetic moment parallel to the magnetic field. By varying the field gradient the complete magnetization of the sample, amplitude and direction, can be determined.

In our design, the sample is placed on a 20-mm-long phosphorbronze wire of  $25\ \mu\text{m}$  diameter, stretched between two epoxy posts, to translate the torque into a rotation  $\phi$  via

$$\Gamma = \left( \frac{\pi R^4 G}{2l} \right) \phi \quad (3.2)$$

where  $R$  is the radius of the wire,  $l$  its length, and  $G$  the torsional spring constant dependent on the material. Using the specified wire a rotation of  $5 \cdot 10^{-6}$  rad/pNm of torque is achieved. The torque wire is glued into a removable part of the magnetometer to allow easy access for sample mounting. Samples with an area up to  $0.64\ \text{cm}^2$  can be accommodated, resulting in a large number of electrons. In this way a high signal-to-noise ratio is achieved.

### **3.2.2 Optical angular detection**

To detect the rotation of the sample, a laser-spot is reflected from it onto a quadrant detector. A 790 nm diode laser is used, with an intensity variable from  $1\ \mu\text{W}$  to  $10\ \text{mW}$ . The laser beam enters the magnetometer through a  $62.5\ \mu\text{m}$  core graded index multimode optical fiber (manufactured by 3M) and is focused on the detector by a 5 mm diameter spherical ball lens, made of the high refractive index material LaSF9. The system can be aligned using two adjustable aluminum mirrors (Fig. 3.1), the first reflecting the incoming light onto the backside of the sample and the second reflecting the light from the sample onto the detector. This detector is a quadrant

detector that consists of four 550  $\mu\text{m}$  core silica/silica multimode fibers connected to four identical silicon diodes. Because optical fibers are used, the diodes can be placed outside the magnetic field at room temperature, making the detection independent of experimental conditions.

As the sample rotates, the movement of the spot changes the intensities  $I_A, I_B, I_C$ , and  $I_D$  in these four fibers ( $A, B, C$ , and  $D$  respectively, see Figure 3.2). The fiber pair  $A$  and  $B$  (as well as the pair  $C$  and  $D$ ) is placed parallel to the torsion wire, perpendicular to the motion of the laser spot. The intensities are translated into a normalized coordinate  $X_{\text{norm}}$  by electronics using low noise amplifiers and analog multipliers, via

$$X_{\text{norm}} = \frac{(I_A + I_B) - (I_C + I_D)}{I_A + I_B + I_C + I_D} \quad (3.3)$$

Note that this coordinate is independent of fluctuations in the total laser intensity. It forms a direct measure of the torque (and therefore through Eq. (3.1) the magnetization) which is linear for moderate rotations of the sample.

The sensitivity of the detector itself is determined by several parameters, most prominently the size of the laser spot and the separation distance between the detector fibers. Sensitivity increases with decreasing spot size and it increases with increasing separation between the fibers. However, at the same time the total detected laser intensity decreases and dynamic range of the detector becomes smaller. Apart from the detector sensitivity, the overall sensitivity can be increased by lengthening the optical path between the sample and the detector, which gives a larger displacement per rotation angle. This has the drawback that the maximum attainable focus for the laser-spot on the detector will be less. In practice a trade-off between available space, the minimally required intensity and laser-spot size has to be made.

We use a separation of 1.0 mm between the detection fibers. The optical path length from the spherical ball lens via the sample to the detector is about 7 cm. A separate determination of the profile of the maximally focussed spot at this distance shows it to be Gaussian with a size of  $\sigma = 0.24$  mm. From these values the response of the quadrant detector can be calculated by integrating the intensity on each of the fiber surfaces for a fixed position of the laser spot.  $X_{\text{norm}}$  follows by inputting the resulting four values in Eq. (3.3). Results of this calculation are plotted by the squares in Figure 3.2. By mounting the 62.5  $\mu\text{m}$  core fiber with



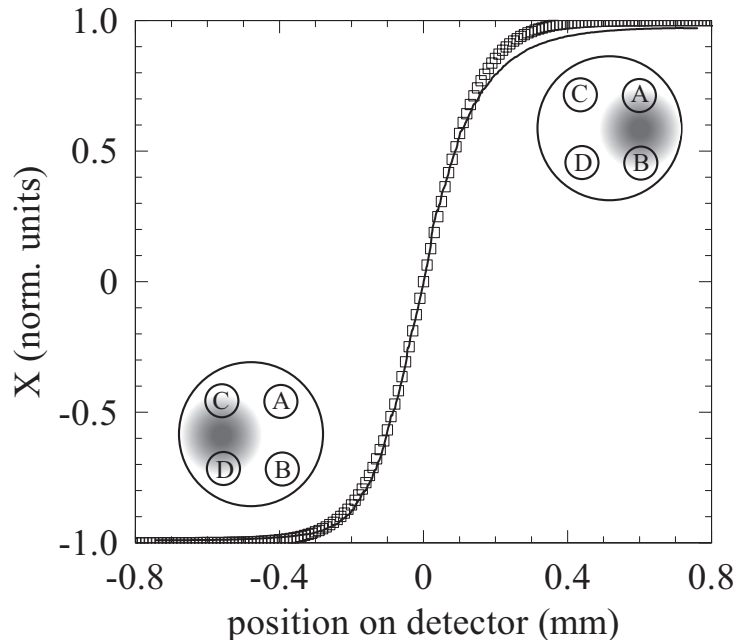


Figure 3.2: Calculated ( $\square$ ) and measured (—) response of the quadrant detector for  $\sigma = 0.24$  mm spotsize and 1.0 mm fiber separation. The position of the laser spot on the detector with the four fibers is depicted left and right. Around zero a displacement by 0.1 mm corresponds to a change in signal of 0.6 normalized units.

the lens and the detector outside the magnetometer, the response of the detector can also be determined experimentally. The position of the detector was varied with high accuracy relative to the (fixed) position of the fiber and lens by a stepmotor controlled translation stage; the measured response is represented by the solid line in Fig. 3.2. As can be seen, the calculated response is in good agreement with the measured response.

Our quadrant detector can resolve rotations as small as  $10^{-7}$  rad, enough to ensure that the detector is not the limiting factor in the sensitivity of the total design.

### 3.2.3 Influence of the laser

While the use of optical detection excludes electronic interference between the sample and the detection, it is necessary to ensure the laser light itself does not have an adverse effect. For example, if the intensity of the laser light is too high, it can increase the temperature of the sample. In order to investigate possible effects of the laser, we make use of the quantum Hall effect. More precisely, we use the Shubnikov-de Haas oscillations in the longitudinal resistance  $R_{xx}$  of a two-dimensional electron gas (2DEG) as a probe. 2DEGs are sensitive to light at the used wavelength of 790 nm: carrier densities can change, and at high enough intensities the temperature of the 2DEG will increase. The quantum Hall effect is sensitive to both these effects: the oscillation period of  $R_{xx}$  depends on the electron density  $n$  and the resistance values of the minima depend on temperature. The sample used is a 7.5 mm  $\times$  7.5 mm piece of GaAs/AlGaAs heterojunction with a Hall-bar etched in the middle, in the position where the laser-spot is reflected on the substrate side.

We determine the effect of the laser illumination at the high intensity of 4.3 mW, by measuring the magnetic field dependence of  $R_{xx}$  at 4.2 K, successively before switching the laser on, while it is on, and after it has been switched off. Figure 3.3 shows the effect of the laser on the 2DEG. Before switching the laser on (dashed line)  $R_{xx}$  oscillates periodically with inverse magnetic field, approaching zero at  $B = 4$  T and 8 T (filling factors 4 and 2). After the laser is switched on (solid line) the carrier density in the 2DEG is increased from the smaller, “dark” value (small dashes) of  $n = 3.8 \cdot 10^{11} \text{ cm}^{-2}$  to a higher saturation value of  $n = 4.3 \cdot 10^{11} \text{ cm}^{-2}$ , as is clear from the higher  $1/B$  frequency of the oscillations and the shift of the minima to  $B = 4.5$  T and 9 T. Illumination usually improves the sample mobility, resulting in deeper minima, but here the minima in  $R_{xx}$  have become less deep. 2DEGs are known to show a parallel conducting channel after illumination (usually in the AlGaAs layer). This parallel conduction short circuits the Hall voltage and causes a small mixture of  $R_{xx}$  with the Hall resistance, resulting in the observed higher resistance values. In magnetization measurements parallel conduction is not relevant, since the contribution of the parallel channel is smooth and shows no oscillatory structure. Comparison of  $R_{xx}$  while the laser is switched on and after it has been switched off (long dashes, Figure 3.3) does not show a change

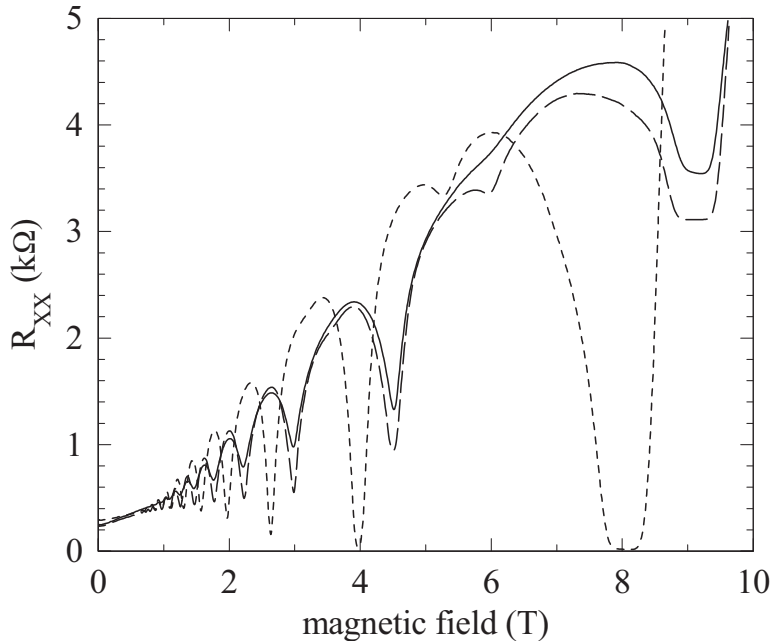


Figure 3.3: Effect of the laser on the sample, determined using the quantum Hall effect at 4.2 K.  $R_{xx}$  was measured before switching the laser on (small dashes), with the laser on at 4.3 mW (solid line), and after the laser is switched off (large dashes).

in density, but the values of the resistance minima are clearly lower after switching the laser off. Our data shows that: i) stray light from the optical detection scheme causes the 2DEG to be fully illuminated, and ii) the laser intensity of 4.3 mW is high enough to heat the sample.

Next, we quantify this heating by measuring the value of the resistance minimum at 6 T (filling factor  $\nu = 3$ , Fig. 3.4(a)) between 4.2 K and 1.2 K. Measuring this value as a function of temperature  $T$  with the laser off provides a calibration of the 2DEG temperature shown in Figure 3.4(b). The parallel conduction is compensated by subtracting a constant value that can be extrapolated from the even  $\nu$  in Fig. 3.4(a), and  $R_{xx}$  of the  $\nu = 3$  minimum shows the typical exponential dependence on  $1/T$  [10]. A fit of the function  $R_{xx} = R_0 \exp(-\Delta/T)$ , shown by the line in Fig. 3.4(b), results in a value of  $\Delta = 0.6$  meV for the energy gap. Although this seems

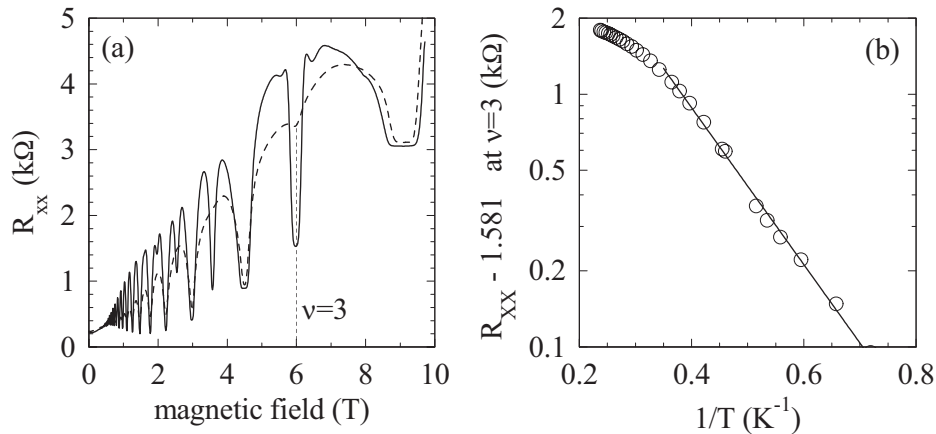


Figure 3.4: Temperature dependence of  $R_{xx}$  at  $\nu = 3$ . (a)  $R_{xx}$  as a function of magnetic field at 4.2 K (dashed line) and 1.2 K (solid line), the minimum at  $\nu = 3$  is clearly deeper at lower temperature. (b) Exponential dependence of  $R_{xx}$  as a function of temperature after subtraction of a constant value to correct for parallel conduction.

rather large, since  $g\mu_B B = 0.15$  meV, the spin gap is usually enhanced by electron-electron interactions (this is further discussed in 4.2.2), and the value we find is reasonable for a spin gap at  $\nu = 3$ .

At a bath temperature of 1.25 K, increasing the intensity of the laser and again measuring the  $R_{xx}$ -minimum at 6 T, allows us to extract the electron temperature as a function of laser power plotted in Figure 3.5. Clearly the 2DEG temperature decreases with decreasing laser intensity, as expected. Below 2 mW the temperature is constant and unaffected by the laser light. The small difference between the value of  $R_{xx}$  with the laser off and with it on at a low intensity is due to a change in the parallel conductance, and is not related to heating. We can conclude that when the laser power input is kept below the value of 2 mW (amply above the value required for the detection electronics) the laser light does not have an unwanted influence on the sample.

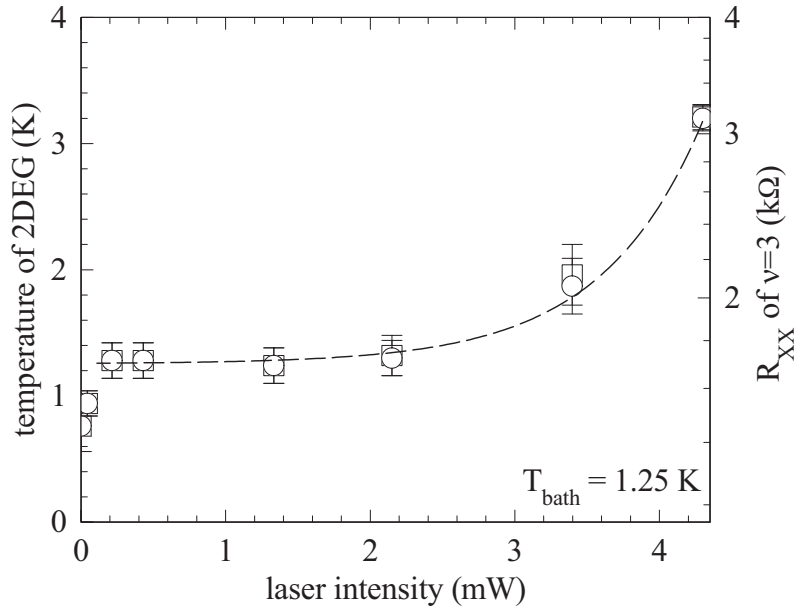


Figure 3.5: Electron temperature, calibrated using  $R_{xx}$  of  $\nu = 3$ , as a function of input laser power (the dashed line is a guide to the eye). The feature at the left is a change in  $R_{xx}$  caused by changing parallel conductance, not increasing temperature. The 2DEG is not heated for intensities below 2 mW.

### 3.2.4 Feedback

Returning to the design of the magnetometer and its detection of a magnetic moment, Figure 3.1 shows how the sample is mounted together with a current coil. This coil allows measurements both in a direct mode and in feedback mode. The feedback coil has a 6 mm diameter and consists of 10 windings of 18  $\mu\text{m}$  Cu wire. In the direct mode the rotation of the sample is measured, and the current coil is only used for *in-situ* calibration. In feedback mode the detector coordinate [Eq. (3.3)] is used as input, and the coil current needed to keep a fixed angle is measured. Operation in feedback mode has two important advantages. First, the fixed angle of the sample with respect to the magnetic field is an advantage in itself. Second, by measuring the feedback current, the magnetization is immediately quantitatively known from the dimensions of the coil.

The magnetometer is normally operated in the feedback mode, and the relevant signal is the DC current required to compensate the rotation induced by the magnetic moment of the sample. Unfortunately, the movement of the sample is also influenced by mechanical noise. Because this noise is the limiting factor in the sensitivity, we take all possible precautions to prevent vibrations from entering the experimental setup. Generally, however, it is necessary to use an active feedback to damp the unwanted additional motion of the magnetometer and it is not sufficient to just filter out the mechanical noise.

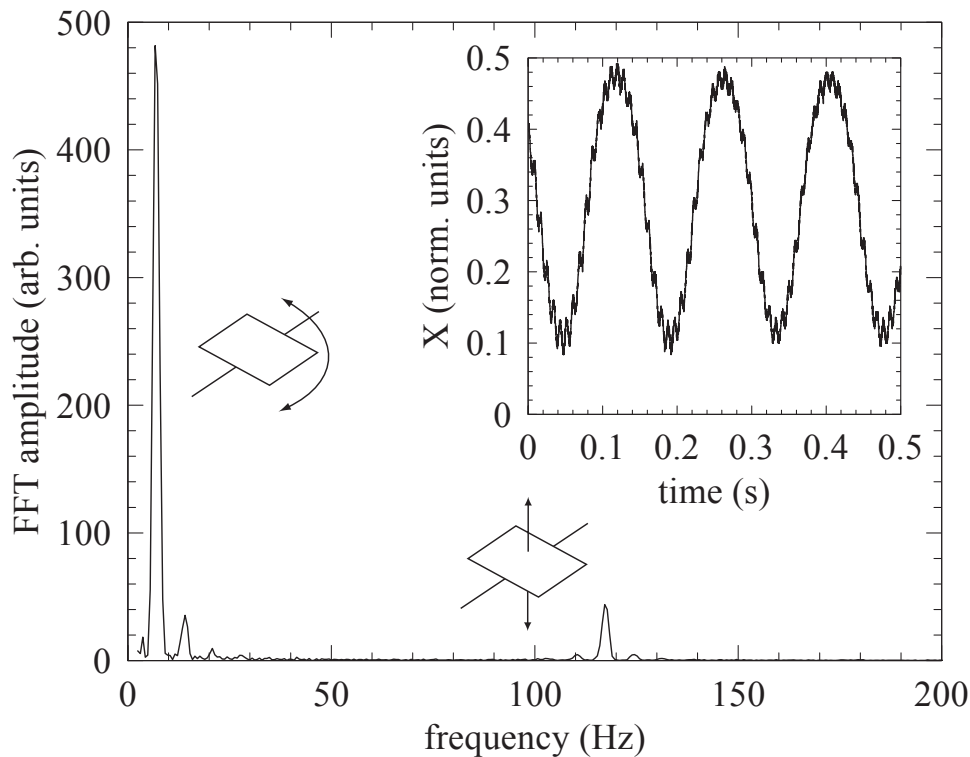


Figure 3.6: Response of the magnetometer to a large, brief input of mechanical noise. Inset shows the motion of the magnetometer with time. The Fourier transform shows the motion to consist of two, sharp frequencies corresponding to the rotational and vibrational eigenmodes (schematically drawn). For the rotational eigenmode (7Hz) small peaks corresponding to higher harmonics are also visible.

The inset of Fig. 3.6 shows a typical response of the magnetometer after the cryostat was briefly hit. Two frequencies corresponding to two eigenmodes of motion are excited (Fig. 3.6). The lower frequency ( $f_1 = 2\pi\omega_1$ ) of 7 Hz is the rotational eigenfrequency of the sample. The highest frequency ( $f_2 = 2\pi\omega_2$ ) of 117 Hz corresponds to vertical vibration of the sample with the torsion wire acting as a string. As is clear from Figure 3.6, the rotational mode is much more easily excited than the vibrational one. The vibrations are usually damped within seconds and not always present. The rotations, however, can take many minutes to dampen and are never completely absent. The active feedback should therefore be aimed at damping this motion.

The feedback current is generated by a proportional-integral-differential controller (PID). The response of such a PID is given by

$$U(t) = G_{\text{prop}} \left( X(t) + \frac{1}{T_I} \int X(t)dt + T_D \frac{d}{dt} X(t) \right) \quad (3.4)$$

where  $U$  is the output voltage of the PID,  $G_{\text{prop}}$  the proportional gain, and  $T_I$  and  $T_D$  are the integral and differential time constants [11]. For a sinusoidal input voltage Eq. (3.4) transforms into the response function

$$\frac{U(\omega)}{X(\omega)} = G_{\text{prop}} \left( 1 + \frac{1}{i\omega T_I} + i\omega T_D \right) \quad (3.5)$$

Considering our input signal consists of the DC component we wish to measure ( $X_M$ ) and two additional AC components with amplitudes  $A_1$  and  $A_2$

$$X_{\text{norm}}(B, t) = X_M(B) + A_1 \sin(\omega_1 t) + A_2 \sin(\omega_2 t), \quad (3.6)$$

we are faced with two problems. First, the gain required to null  $X_M$  is different from the optimal gain for the AC feedback. Second, as is clear from Eq. (3.5), when the feedback is optimized for  $\omega_1$ , there is a phase shift at the higher  $\omega_2$  large enough to cause  $A_2$  to be enhanced instead of reduced. To set the optimal gain, the signal  $X_{\text{norm}}(B, t)$  is split into its DC part, by using a low-pass filter, and an AC part. Both are amplified by an appropriate factor. Equations 3.1 and 3.2 show that for fixed current in the coil (fixed  $\mathbf{M}$ ) rotation increases linearly with magnetic field, and the AC signal is therefore divided by  $B$  to keep the gain constant. Since the vibrational eigenmode ( $\omega_2$ ) is naturally small and damps quickly, we

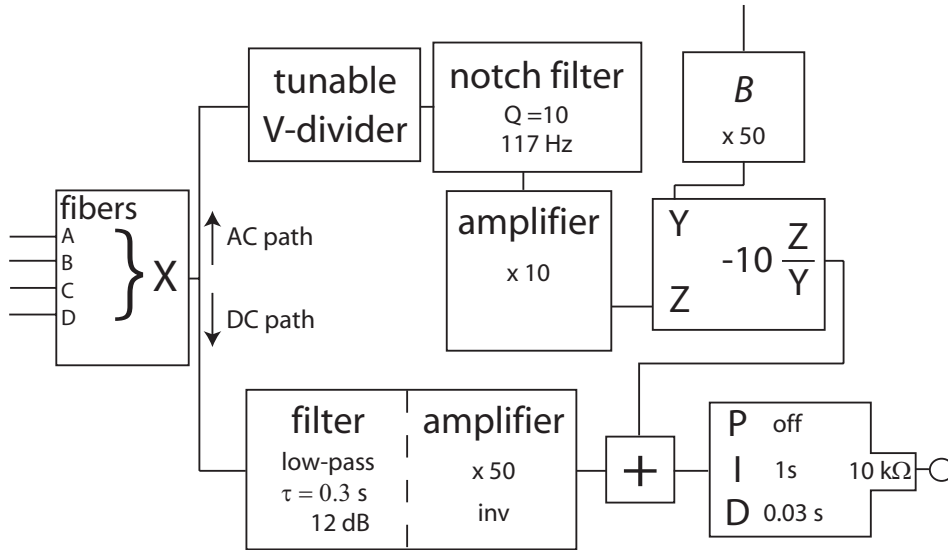


Figure 3.7: Schematic representation of the electronic feedback circuit. The position signal of the detector is filtered and amplified in two separate AC and DC paths, the outputs of which are added and used as input for PID which provides the current sent into the feedback loop.

solve the problem of amplifying  $A_2$  by filtering out this component from the AC part of the signal using a notch filter before adding the result to the DC part to provide the total signal that enters the PID. A schematic representation of the feedback circuit as realized in practice, with typical values of the different parameters, is shown in Fig. 3.7.

### 3.3 Application of the technique

To demonstrate the performance of the setup, we have investigated the magnetization of two distinctly different physical systems: an organic crystal and a semiconductor heterostructure, in the operating environments of a superconducting magnet and a Bitter-magnet.



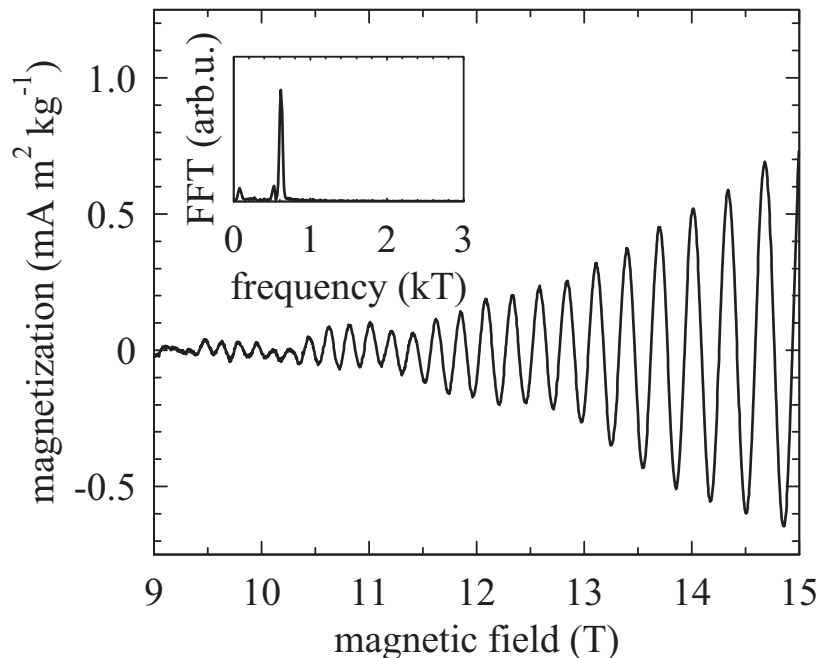


Figure 3.8: Magnetization of  $\kappa$ -(BEDT-TTF) $_2$ Cu(NCS) $_2$  at 1.2 K after subtraction of a small, smooth background. The inset shows the usual Fourier analysis of the magnetization. A sharp peak occurs at a frequency of 617 T.

### 3.3.1 Magnetization of $\kappa$ -(BEDT-TTF) $_2$ Cu(NCS) $_2$

The magnetization of a 130  $\mu$ g crystal of  $\kappa$ -(BEDT-TTF) $_2$ Cu(NCS) $_2$  was measured at 1.2 K. It is a well-known compound that shows large de Haas-van Alphen oscillations at this low temperature.  $\kappa$ -(BEDT-TTF) $_2$ Cu(NCS) $_2$  is an organic superconductor with a critical temperature of  $T_c = 10$  K and a highly anisotropic electronic structure: electrons in the crystal show quasi-two-dimensional behavior. The sample used here is a platelet of irregular shape, mounted with angle of  $\theta = 13^\circ \pm 1^\circ$  between the applied magnetic field and the normal to the platelet, which is the normal to the plane of conduction. A thin glass plate coated with a layer of Al is used as a sample-mounting platform for maximum reflection of

the laser beam. Figure 3.8 shows the magnetization<sup>1</sup> of the  $\kappa$ -(BEDT-TTF)<sub>2</sub>Cu(NCS)<sub>2</sub>. It exhibits large oscillations periodic in  $B^{-1}$ . A smooth curve was subtracted from the data to account for the background magnetization due to the sample-mounting platform. The Fourier analysis shows a sharp peak at a frequency of 617 T, which is in agreement with the value of 601 T/cos $\theta$  found in other works [12–15].

The measurements were performed in a superconducting magnet, where the sensitivity of the magnetometer is limited by mechanical noise. Data points are typically taken at a rate of one per second, the active feedback damps any additional vibrations well within this time. In this environment the sensitivity increases linearly with the magnetic field as expected from Equations (3.1) and (3.2), which show that the rotation of a constant magnetic moment increases linearly with the magnetic field. With the constant noise level this results in the observed linear increase of sensitivity. The value is determined from the width of the noise band and is  $2 \cdot 10^{-13}$  J/T at 15 T.

### 3.3.2 Magnetization of a 2D electron system

As was introduced in chapter 2.3.3, for a 2DEG changes in the magnetization are directly proportional to changes in the chemical potential. Magnetometry is therefore a particularly useful tool, since it gives direct access to the size as well as the shape of the Fermi energy (i.e. the way the Fermi energy varies with magnetic field). The measured sample is a 7.7 mm $\times$ 5.0 mm GaAs/AlGaAs heterostructure, which was grown by molecular beam epitaxy [16]. The 2DEG in this structure has an electron density of  $n = 8.0 \cdot 10^{11}$  cm<sup>-2</sup>, which is high enough to occupy two electronic subbands. The substrate side of the sample was polished for reflection, and for the measurements it was mounted directly on the wire. Because a sample-mounting platform is not needed, the background magnetization is reduced to a minimum. This background is a smooth function, about 50 times larger than the magnetization of the 2DEG, which means the sharp de Haas-van Alphen oscillations can immediately be distinguished.

---

<sup>1</sup>The irregular shape of this type of sample means the mass can be determined more precisely than the volume. The magnetization is therefore expressed in magnetic moment per unit of mass instead of volume.

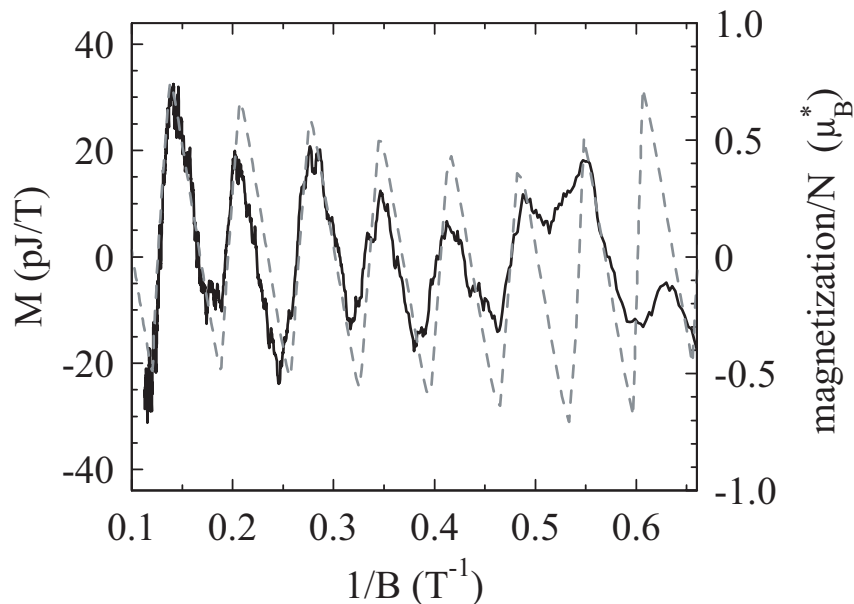


Figure 3.9: Magnetization of a 2DEG with two filled electronic subbands ( $n = 8.0 \cdot 10^{11} \text{ cm}^{-2}$ ) at 4.2 K in a Bitter-magnet. A smooth curve was subtracted from the data to correct for the diamagnetic contribution of the GaAs substrate. The dashed line is a self-consistent calculation at 0 K.

Figure 3.9 shows the magnetization of the multi-subband 2DEG at 4.2 K, measured in a Bitter-magnet. For our experiments we typically use sweep rates for the magnetic field between 0.2 T/min and 1.0 T/min; for the measurements shown in Fig. 3.9 a rate of 0.3 T/min was used. The left axis of the graph corresponds to the measured total magnetic moment, the right axis shows the magnetization<sup>2</sup> normalized to the number of electrons  $N$  in the 2DEG. The sensitivity of  $2 \cdot 10^{-13} \text{ J/T}$  at 15 T that is achieved when the system is operated in a superconducting magnet (see 3.3.1), corresponds to a resolution of  $5 \cdot 10^{-3} \mu_B^*$  per electron. However, in a Bitter-magnet the sensitivity is reduced due to field noise. Because this

<sup>2</sup>We conform to the commonly used definition used by Shoenberg [17](chapter 2.3.2), where the magnetization of a 2DEG is that of the entire collection of  $N$  electrons. The magnetization is then equal to the magnetic moment.

field noise increases with increasing magnetic field, the sensitivity remains more or less constant as a function of the applied field. A sensitivity of  $10^{-12}$  J/T is reached, giving a resolution of  $0.02 \mu_B^*$  per electron, enough to give a good resolution of the typically small signal.

The magnetization oscillates in a triangularly shaped manner as a function of the magnetic field. This behavior has not been observed previously and is typical for an electron system in a heterojunction with two filled electronic subbands as opposed to 2DEGs with a single filled subband, where the magnetization is a sawtooth. In order to understand this behavior, we have calculated the Fermi energy at 0 K, where it is exactly equal to the chemical potential. Since in a heterostructure the confining potential, the subband occupation and Fermi level are interdependent, the Schrödinger equation and the Poisson equation have to be solved self-consistently [18] (this system is extensively discussed in chapter 5). It can be seen in Fig. 3.9 that the model reproduces the most prominent features of the data.

Because magnetometry gives direct access to a thermodynamic property of the 2DEG, much effort has been put into the development of a magnetometer that is sensitive enough to measure its magnetization. However, since the size of the magnetization scales directly with the surface area of the sample, it is not the absolute sensitivity that is important, but the resolution of sensitivity per electron that can be achieved. Torsional magnetometers capable of supporting larger samples with sizes of a few  $\text{mm}^2$  have been used before [4–7], but the resolution achieved was significantly less than  $5 \cdot 10^{-3} \mu_B^*$  per electron. Also, these designs all make use of a capacitive detection method, without the possibility for feedback. Capacitive coupling of the 2DEG with the detection is a known problem [19, 20] that cannot occur in our optical detection. By using the feedback mode, we make a direct, quantitative measurement, while keeping the angle of the sample with respect to the magnetic field constant. More recently, other magnetometers, a superconducting quantum interference device (SQUID) [21] and a cantilever [3], have also been developed for measurements on the 2DEG in GaAs/AlGaAs structures. The SQUID provides very high sensitivity at low values of the magnetic field, but the sensitivity decreases rapidly with increasing magnetic field, and the device can only be used up to 10 T. This technique is thus complementary to torsional magnetometry, rather than a substitute. Although the sensitiv-

ity of the cantilever is nearly an order of magnitude higher, the maximum sample area is more than an order of magnitude smaller, resulting in a resolution that is less than  $5 \cdot 10^{-3} \mu_B^*$  per electron, but comparable to the resolution we achieve when operating the system in a Bitter-magnet.

### 3.4 Conclusion

We have developed a multipurpose, sensitive torsional magnetometer with optical angular detection that is capable of supporting large samples. The use of feedback gives a direct, quantitative measurements of the magnetization. To demonstrate the versatility and sensitivity, we presented de Haas-van Alphen measurements of  $\kappa$ -(BEDT-TTF)<sub>2</sub>Cu(NCS)<sub>2</sub> and of a 2DEG with multiple filled subbands. The magnetometer was found to have a sensitivity of  $2 \cdot 10^{-13}$  J/T at 15 T, giving a resolution of  $5 \cdot 10^{-3} \mu_B^*$  per electron.

### 3.5 Acknowledgments

We thank W. Biberacher for stimulating discussions and for providing the  $\kappa$ -(BEDT-TTF)<sub>2</sub>Cu(NCS)<sub>2</sub> sample. We would also like to thank A.K. Geim for useful discussions and continued interest in this work.

### References

- [1] M. Chaparala, O. H. Chung, and M. J. Naughton, AIP conf. proc. **273**, 407 (1992).
- [2] J. S. Brooks, M. J. Naughton, Y. P. Ma, P. M. Chaikin, and R. V. Chamberlin, Rev. Sci. Instrum. **58**, 117 (1987).
- [3] M. P. Schwarz, D. Grundler, I. Meinel, C. Heyn, and D. Heitmann, Appl. Phys. Lett. **76**, 3564 (2000).
- [4] J. P. Eisenstein, Appl. Phys. Lett. **46**, 695 (1985).
- [5] I. M. Templeton, J. Appl. Phys. **64**, 3570 (1988).

- 
- [6] S. A. J. Wieggers, M. Specht, L. P. Lévy, M. Y. Simmons, D. A. Ritchie, A. Cavanna, B. Etienne, G. Martinez, and P. Wyder, *Phys. Rev. Lett.* **79**, 3238 (1997).
- [7] P. A. Crowell, A. Madouri, M. Specht, G. Chaboussant, D. Maily, and L. P. Lévy, *Rev. Sci. Instrum.* **67**, 4161 (1996).
- [8] S. A. J. Wieggers, A. S. van Steenbergen, M. E. Jeuken, M. Bravin, P. E. Wolf, G. Remenyi, J. A. A. J. Perenboom, and J. C. Maan, *Rev. Sci. Instrum.* **69**, 2369 (1998).
- [9] J. G. E. Harris, D. D. Awschalom, F. Matsukura, H. Ohno, K. D. Maranowski, and A. C. Gossard, *Appl. Phys. Lett.* **75**, 1140 (1999).
- [10] T. Chakraborty and P. Pietiläinen, in *The Quantum Hall Effects*, Vol. 85 of *Solid State Sciences*, edited by M. Cardona, P. Fulde, K. von Klitzing, and H.-J. Queisser (Springer, Heidelberg, 1995).
- [11] D. Blok, C. L. Doesburg, and R. Y. Drost, *Elektronisch vademecum: handleiding voor de moderne elektronica*, 2e ed. (Kluwer, Deventer, 1968).
- [12] A. Swanson, J. Brooks, H. Anzai, N. Konoshita, M. Tokomuto, and K. Murata, *Solid State Commun.* **73**, 353 (1990).
- [13] P. van der Wel, J. Caulfield, R. Corcoran, P. Day, S. Hayden, W. Hayes, M. Kurmoo, P. Meeson, J. Singleton, and M. Springford, *Physica B* **235-240**, 2453 (1994).
- [14] F. Meyer, E. Steep, W. Biberacher, P. Christ, A. Lerf, A. Jansen, W. Joss, P. Wyder, and K. Andres, *Europhys. Lett.* **32**, 681 (1995).
- [15] C. Lupien, B. Ellman, P. Grütter, and L. Taillefer, *Appl. Phys. Lett.* **74**, 451 (1999).
- [16] D. Reuter, M. Versen, M. D. Schneider, and A. D. Wieck, *J. Appl. Phys.* **88**, 321 (2000).
- [17] D. Shoenberg, *Magnetic oscillations in metals*, *Cambridge monographs on physics* (Cambridge University Press, Cambridge, 1984).

*A multipurpose torsional magnetometer with optical angular detection*

- [18] M. R. Schaapman, U. Zeitler, P. C. M. Christianen, J. C. Maan, D. Reuter, A. D. Wieck, D. Schuh, and M. Bichler, Phys. Rev. B **68**, 193308 (2003).
- [19] I. M. Templeton, J. Appl. Phys. **62**, 4005 (1987).
- [20] S. A. J. Wiegers, J. C. Maan, and C. T. Foxon, Physica B **211**, 474 (1995).
- [21] I. Meinel, D. Grundler, S. Bargstädt-Franke, C. Heyn, D. Heitmann, and B. David, Appl. Phys. Lett. **70**, 3305 (1997).

# Chapter 4

## Magnetization of a two-dimensional electron gas

### Abstract

We have measured the magnetization of a single 2DEG and observe the expected, saw-tooth shaped,  $\nu$ -periodic de Haas-van Alphen oscillations. The amplitude of the oscillations increases with decreasing temperature, and at even  $\nu$ , corresponding to Landau-level transitions, it saturates to the anticipated  $1 \mu_B^*$  per electron. Contrary to the calculated saw-tooth, the steps in the magnetization have a small, but finite width attributed to the presence of a background density of states. Additionally, at 1.2 K, we observe shoulders at  $\nu = 3$ , and 5, suggesting a spin-gap enhanced by many-body interactions.

### 4.1 Introduction

While the two-dimensional electron gas (2DEG) in semiconductor structures is one of the most widely studied systems in condensed matter

---

Part of this work has been published in:

M. R. Schaapman, U. Zeitler, P. C. M. Christianen, J. C. Maan, D. Reuter, A. D. Wieck, D. Schuh, and M. Bichler, Phys. Rev. B **68**, 193308 (2003).



physics, only very few experiments are able to directly probe a thermodynamic property of the 2DEG. The reason lies in the difficulty of measuring the tiny signal originating from the 2DEG in experiments like specific heat [1] and magnetization [2–4] measurements.

We study the magnetization ( $M$ ) of the 2DEG, which is only  $1 \mu_B^*$  per electron in size. Measuring the magnetization is a way of directly probing the chemical potential ( $\mu$ ).  $M$  and  $\mu$  are related via a Maxwell relation that states that changes in  $M$  are directly proportional to changes in  $\mu$ , and therefore the shape of  $\mu$  can be seen immediately from the shape of  $M$ . Magnetization is also the derivative of the free energy ( $F$ ), which for a 2DEG of area  $A$  and a fixed number of electrons  $N$ , using Fermi-Dirac statistics, can be written as

$$F = \mu N - kTA \int D(E) \ln \left[ 1 + \exp \left( \frac{\mu - E}{kT} \right) \right] dE \quad (4.1)$$

as we have already seen in Eq. (2.10) of chapter 2.3.2. In other words, by measuring  $M$  we can probe the shape of the density of states ( $D(E)$ ,  $E$  is the internal energy).

The subject of this chapter is the magnetization of the 2DEG consisting of only one component: the single layer 2DEG with one filled electronic subband. Due to its relative simplicity, it is a good model system, and yet it shows interesting features related to single-particle as well as many-body physics. We will see that the magnetization shows the well-known  $\nu$ -periodic, saw-tooth shaped de Haas-van Alphen oscillations with an amplitude of  $1 \mu_B^*$  per electron (chapter 2.3.2) [3, 5], demonstrating the ability of our setup (chapter 3) to make an immediate, quantitative determination of  $M$ . Interestingly, however, the steps of the saw-tooth are not infinitely sharp. We will relate this finite step width to the presence of a background density of states (DOS) in between the Landau-levels. Additionally we observe features related to spin-splitting, enhanced by many-body interactions.

## 4.2 Magnetization of the single layer, single subband 2DEG

The 2DEG used to investigate the magnetization is realized in a GaAs/AlGaAs heterojunction grown by molecular beam epitaxy. The sample has a density of  $n = 4.8 \cdot 10^{11} \text{ cm}^{-2}$ , and a mobility of  $2.2 \cdot 10^6 \text{ cm}^2/\text{Vs}$ . At this density only one subband of the system is occupied. The measurements were done by using the torsional magnetometer with optical angular detection, described in chapter 3 [6].

Figure 4.1 shows the magnetization of the single component 2DEG as a function of filling factor ( $\nu = hn/eB$ , where  $B$  is the magnetic field). It displays de Haas-van Alphen oscillations, periodic in  $\nu$ . In fact, as Figure 4.1(b) shows most clearly, the magnetization has two different types of alternating periodic features.

### 4.2.1 Landau-level transitions

The observed steps at even filling factors correspond to magnetic fields where the Fermi energy jumps across a Landau-gap. Comparison of Figures 4.1(a) and (b), measured at 4.2 K, and 1.2 K respectively, shows that both the oscillation amplitude and the sharpness of the steps increase with decreasing temperature. While at 4.2 K the last oscillation is observed at  $\nu = 10$ , at 1.2 K oscillations can be observed up to  $\nu = 14$ . This behavior can be easily understood by considering the exponential temperature dependence given by Fermi-Dirac statistics in Eq. (4.1). At the lowest of the even filling factors, where Landau-level broadening has the least influence, the steps are saw-tooth shaped. With decreasing temperature the amplitude of this saw-tooth saturates to the expected  $1 \mu_B^*$  per electron.

While the amplitude and periodicity of the observed de Haas-van Alphen oscillations correspond to the well-known  $1 \mu_B^*$  saw-tooth we have seen in chapter 2.3.2, the actual step at the transition shows some discrepancy. Although the steps are rather sharp, even at 1.2 K they still have a small, finite width. This width is attributed to a finite, background DOS in between Landau-levels [3, 7]. An extensive investigation of this background DOS at much lower temperatures, where more sharp steps are observed, has been made by Schwarz et al. [7]. The authors find that a

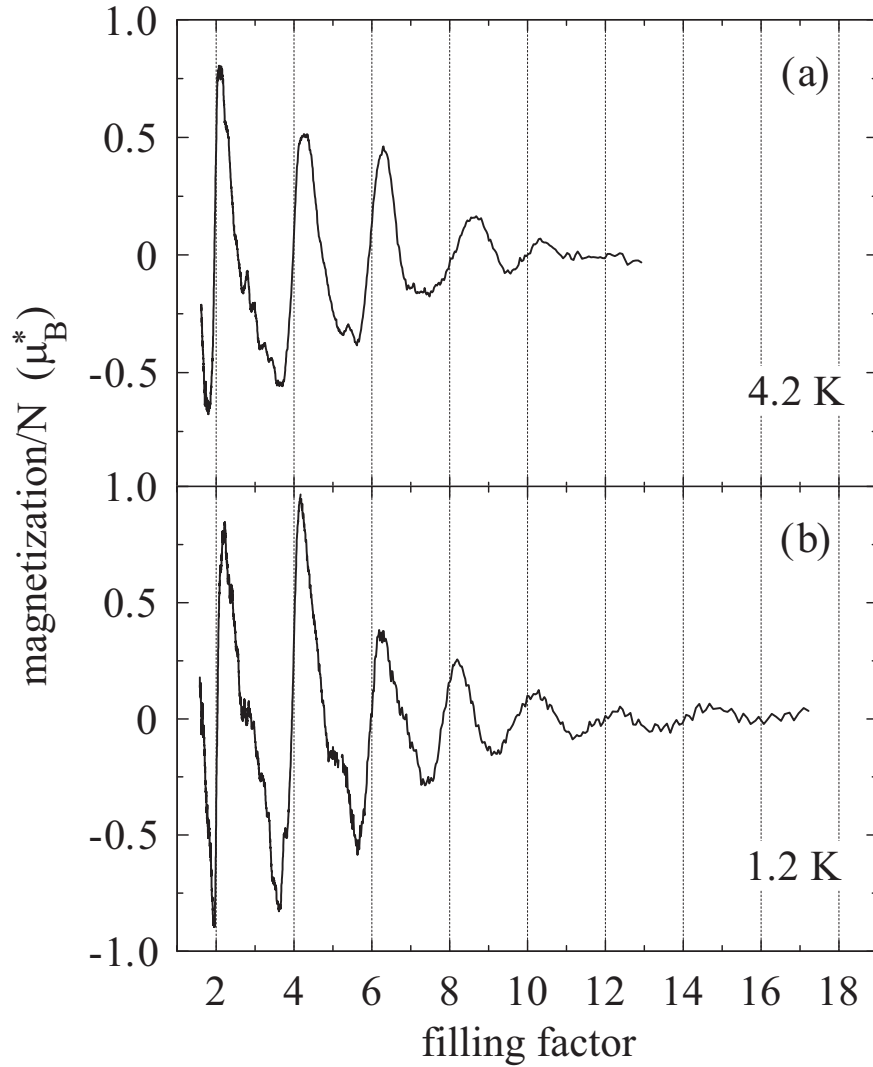


Figure 4.1: Magnetization of sample 1 (single 2DEG with  $n = 4.8 \cdot 10^{11} \text{ cm}^{-2}$ ) at 4.2 K (a) and 1.2 K (b). Oscillations are a strictly  $1/B$ -periodic saw-tooth, the amplitude saturates to  $1 \mu_B^*$  per electron at low  $\nu$ . Features at filling factors 3 and 5 are related to enhanced spin-splitting.

model DOS given by

$$D(E) = xD_0 + (1-x) \frac{2n}{\nu} \sum_j \frac{1}{\sqrt{2\pi}\Gamma} \exp \left[ -\frac{(E - E_j)^2}{2\Gamma^2} \right] \quad (4.2)$$

used in Eq. (4.1), provides a good fit to their magnetization data. Here  $x$  represents the fraction of states forming the background, and  $D_0 = m^*/\pi\hbar^2$  is the DOS at 0 T. The Landau levels  $E_j$  have Gaussian broadening with width  $\Gamma$ .

At our experimental temperature only two features ( $\nu = 2$ , and 4) are fully developed, and we therefore use the approach by Wiegers et al. [3] to estimate the number of states in the gap ( $N_{\text{gap}}$ ) via  $N_{\text{gap}} = N\Delta B/B$ , where  $\Delta B$  is the width of the step and  $B$  the magnetic field at which it occurs. We find a background DOS of 4.7% at  $\nu = 4$  and 10% at  $\nu = 2$ . These values are in agreement with magnetization measurements where samples of similar mobility were used and are in reasonable correspondence with the linear increase of the background DOS with  $\nu$  found by Schwarz et al. [3, 7].

### 4.2.2 Enhanced spin-splitting

Apart from the clear steps assigned to the Landau gap at even integer filling factors, at 1.2 K (Figure 4.1(b)) additional features appear at odd integer filling factors ( $\nu = 3$ , and 5). They are attributed to transitions of the Fermi energy across a spin-gap. The observation of the shoulders at  $\nu = 3$ , and 5 suggest the gap is significantly larger than the single-particle gap of  $g\mu_B B = 25 \mu\text{eV} \times B$  ( $g = -0.44g_0$ ), since this would be below the detection limit. Enhancement of the gap is due to exchange interaction [4, 8, 9], and in a 2DEG it is commonly described by [10]:

$$E_s = g\mu_B^* B + E_C \left( \frac{N_\uparrow - N_\downarrow}{N_{\text{total}}} \right) \quad (4.3)$$

with  $E_C$  the Coulomb energy and  $N_{\uparrow,\downarrow}$  the number of electrons with spin up and down respectively<sup>1</sup>. Equation (4.3) suggests that a spin-polarized state is energetically favored by the 2DEG. Hence the enhancement is largest precisely at the transitions (odd  $\nu$ ) and increases with increasing magnetic field (decreasing  $\nu$ ). An equivalent way of describing Eq. (4.3),

---

<sup>1</sup>The observation of a change in the spin-magnetization, which is in principle isotropic, is interesting in itself, as our setup, as used here, is only sensitive to anisotropic magnetic moments. The enhancement, however, depends on the population of the energy-levels and thereby on the *perpendicular* magnetic field, making the magnetic moment anisotropic and observable.

is to say the system has a larger, effective  $g$ -factor which is an oscillatory function of magnetic field.

The experimentally observed magnetization of the 2DEG (fig. 4.1b) corresponds to these facts. We only observe spin-related features at the lowest odd filling factors, corresponding to the highest magnetic fields.

### 4.3 Conclusion

We have determined the magnetization of a single component 2DEG. The measured magnetization shows the well known, saw-tooth shaped,  $\nu$ -periodic oscillations. The amplitude of the oscillations increases with decreasing temperature, and at even  $\nu$ , corresponding to Landau-level transitions, it saturates to the expected  $1 \mu_B^*$  per electron.

We find, however, the steps in the magnetization have a small, but finite width not present in the calculated saw-tooth. This width is attributed to the presence of a background DOS, also observed by others [3, 7]. Additionally, at 1.2 K, we observe shoulders at  $\nu = 3$ , and 5, indicating the spin-gap is enhanced by many-body interactions.

### References

- [1] E. Gornik, R. Lassning, G. Strasser, H. L. Störmer, and W. Wegmann, Phys. Rev. Lett. **54**, 1820 (1985).
- [2] J. P. Eisenstein, H. L. Stormer, V. Narayanamurti, A. Y. Cho, A. Gossard, and C. W. Tu, Phys. Rev. Lett. **55**, 875 (1985).
- [3] S. A. J. Wieggers, M. Specht, L. P. Lévy, M. Y. Simmons, D. A. Ritchie, A. Cavanna, B. Etienne, G. Martinez, and P. Wyder, Phys. Rev. Lett. **79**, 3238 (1997).
- [4] I. Meinel, T. Hengstmann, D. Grundler, D. Heitmann, W. Wegscheider, and M. Bichler, Phys. Rev. Lett. **82**, 819 (1999).
- [5] D. Shoenberg, *Magnetic oscillations in metals*, Cambridge monographs on physics (Cambridge University Press, Cambridge, 1984).

- [6] M. R. Schaapman, P. C. M. Christianen, J. C. Maan, D. Reuter, and A. D. Wieck, *Appl. Phys. Lett.* **81**, 1041 (2002).
- [7] M. P. Schwarz, M. A. Wilde, S. Groth, D. Grundler, C. Heyn, and D. Heitmann, *Phys. Rev. B* **65**, 245315 (2002).
- [8] R. J. Nicholas, R. J. Haug, and K. von Klitzing, *Phys. Rev. B* **37**, 1294 (1988).
- [9] D. Grundler, I. Meinel, S. Bargstädt-Franke, and D. Heitmann, *Physica B* **249-251**, 693 (1998).
- [10] T. Englert, D. C. Tsui, A. C. Gossard, and C. Uihlein, *Surf. Sci.* **113**, 295 (1982).



# Chapter 5

## Magnetization of a two-dimensional electron gas with a second filled subband

### Abstract

We have measured the magnetization of a dual-subband two-dimensional electron gas, confined in a GaAs/AlGaAs heterojunction. Contrary to two-dimensional electron gases with a single subband, we observe non- $1/B$ -periodic, triangularly shaped oscillations of the magnetization with an amplitude significantly less than  $1\mu_B^*$  per electron. All three effects are explained by a field-dependent self-consistent model, demonstrating that the shape of the magnetization is dominated by oscillations in the confining potential. Furthermore, at 1 K, we observe small oscillations at magnetic fields where Landau levels of the two different subbands cross.

---

Part of this work has been published in:

M. R. Schaapman, U. Zeitler, P. C. M. Christianen, J. C. Maan, D. Reuter, A. D. Wieck, D. Schuh, and M. Bichler, Phys. Rev. B **68**, 193308 (2003).



## 5.1 Introduction

When an extra degree of freedom is added to a two-dimensional electron gas (2DEG), many-body interactions can lead to the formation of novel electronic ground states at the crossings of the different energy levels in the system [1]. Two-dimensional electron gases with crossing energy levels can be realized in a variety of systems with different relative sizes of orbital and spin effects, Coulomb energy, and different coupling between the components. Their study has led to the discovery of many correlated quantum Hall states [2–4], and much effort is put into unravelling the energy-level structure of these systems.

One way of realizing such a 2D system, is to increase the electron density of a III-V 2DEG such that a second subband becomes occupied. Dual-subband systems realized in a quantum well have recently been studied within this context [5, 6]. A similar system is the dual-subband 2DEG in a GaAs/AlGaAs heterojunction.

In transport studies, the multisubband 2DEG is generally assumed to be a superposition of single 2DEGs: the Landau-level structure is a superposition of Landau fans, separated by the intersubband spacing calculated self-consistently at zero magnetic field [7, 8].

In this chapter we study the magnetization  $M$  of a dual-subband 2DEG. This is a way to directly probe a thermodynamic property, the chemical potential  $\mu$ . For two-dimensional systems, the Maxwell relation between  $M$  and  $\mu$  is reduced to a proportionality. Since the Fermi energy  $E_F$  is equal to  $\mu$  at low temperatures, the magnetization directly reveals changes in the size as well as the shape (i.e. the way it varies with magnetic field) of the Fermi energy, as we have seen in chapter 2:  $\Delta M = (N/B)\Delta E_F$ , where  $N$  is the total number of electrons.

The magnetization of multisubband 2DEGs has already attracted some attention, both theoretically [9, 10] and experimentally [11]. However, these studies have focussed on very high-density systems with three or more filled subbands. In this regime changes in the energy gap between the subbands can be ignored. We focus on the effect of the filling of only a second electronic subband on the Fermi energy.

As we have seen in chapter 4, quantum oscillations in the magnetization of a single 2DEG are characterized by strictly  $1/B$ -periodic sawtoothlike oscillations with an amplitude of 1 effective Bohr magneton ( $\mu_B^*$ )

per electron [12–14]. Here we show that this is no longer the case in our multi-component system. Due to a self-consistent, magnetic-field dependent redistribution of electrons between the subbands inside the heterojunction, the amplitude of the oscillations becomes considerably reduced, the sawtoothlike steps are broadened into triangles, and the  $1/B$  periodicity is lost. Additionally we find that extra magnetization minima appear at low temperature at the Landau-level crossings of the two subbands.

## 5.2 Experimental results

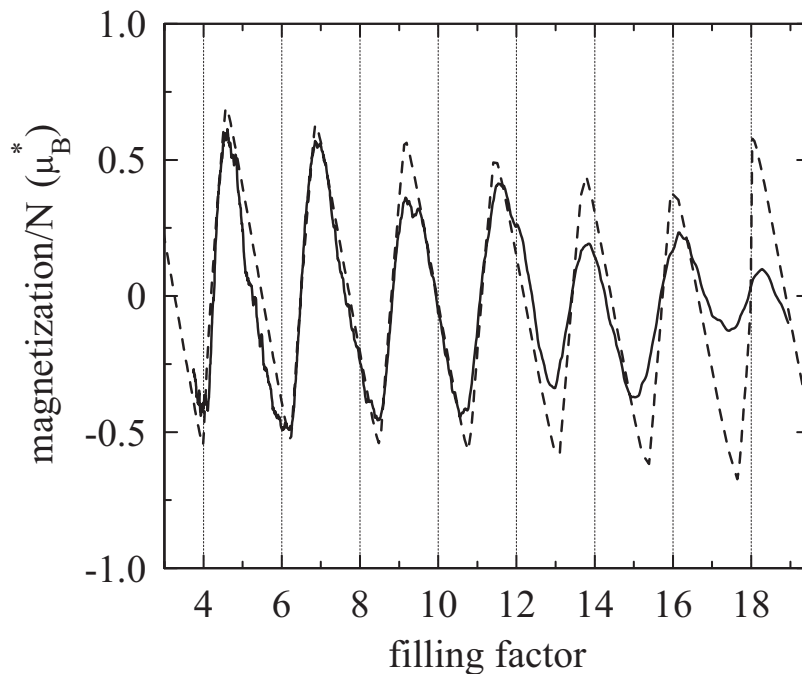


Figure 5.1: Magnetization of the dual-subband 2DEG with  $n = 8.0 \cdot 10^{11} \text{ cm}^{-2}$  at 4.2 K. The dashed line is a self-consistent calculation using a Gaussian Landau-level broadening with  $\Gamma = 0.2\sqrt{B}$  meV. Note the deviation from  $1/B$ -periodicity and the reduced amplitude of about  $0.5\mu_B^*$  per electron.

We study a high electron density 2DEG, realized in a GaAs/AlGaAs

heterojunction grown by molecular-beam epitaxy. Our sample has a carrier concentration of  $8.0 \times 10^{11} \text{ cm}^{-2}$  (high enough for a second subband to be filled), and a mobility of  $1.4 \times 10^6 \text{ cm}^2/\text{Vs}$ . Most of the electrons ( $7.4 \times 10^{11} \text{ cm}^{-2}$ , deduced from transport measurements on a reference sample) remain in the lowest subband; the small remaining fraction occupies the second subband. The magnetization experiments were performed with the torsional magnetometer with optical angular detection [15] described in chapter 3.

The dual-subband 2DEG displays the magnetization plotted by the solid line in Figure 5.1. The magnetization here also oscillates as a function of inverse magnetic field, similar to the single subband 2DEG presented in chapter 4. Closer inspection of the data, however, reveals three distinct differences. First, the oscillations are no longer sawtoothlike, but instead they are triangular. Second, we find that the oscillations are no longer strictly periodic in  $1/B$ . Note for example that  $\nu = 4$  coincides with an oscillation minimum, while  $\nu = 14$  actually coincides with an oscillation maximum. Finally, the amplitude of the oscillation is about  $0.5\mu_B^*$  per electron, even at low temperatures (see Fig. 5.5) and for the lowest filling factors, instead of the  $1\mu_B^*$  per electron observed in Figure 4.1 for the single 2DEG.

### 5.3 Self-consistent field-dependent model

In order to understand the behavior of the magnetization, it is important to realize that in a heterojunction most of the confining potential of the 2DEG is formed by the electrons themselves. In a dual-subband 2DEG redistribution of charge over the two subbands can occur when a magnetic field is applied, resulting in a potential that is not fixed as a function of magnetic field. The wave function of the second subband is much more extended than that of the first one, and therefore even a small change in its occupation can have profound effects. Since the occupation of the two subbands depends on the magnetic field that quantizes the density of states (DOS) into Landau levels, and since the shape of the confining potential, the intersubband spacing, and the spatial charge distribution are interdependent, the Schrödinger and Poisson equations have to be solved self-consistently (chapter 2.2.2) for each value of the magnetic field [16, 17].

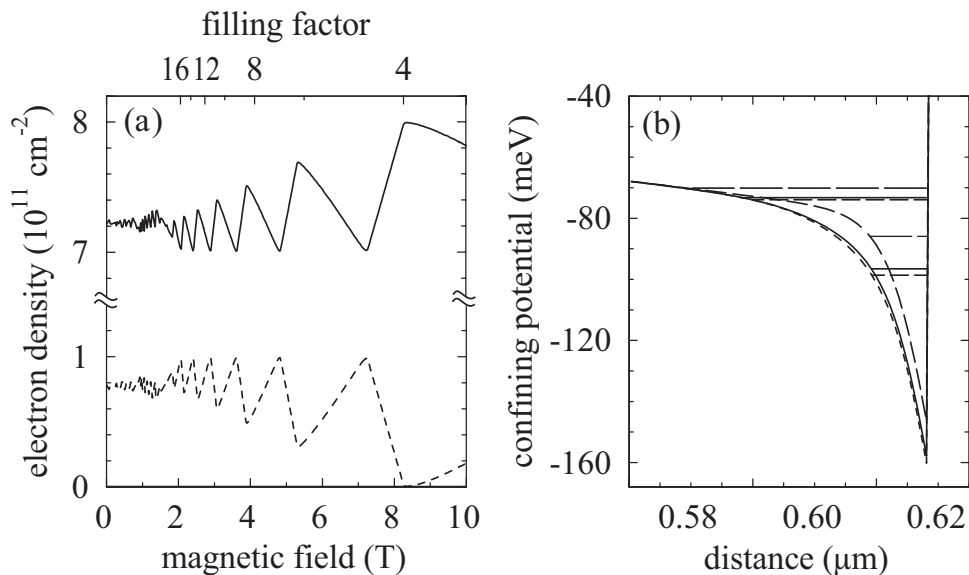


Figure 5.2: Field-dependent, self-consistent calculations of (a) the populations of the first (solid line) and second (dashed line) subband, and (b) the confining potential. The confining potential is calculated relative to the GaAs conduction band at 0.0 T (solid line), 4.8 T (small dashes) and 8.3 T (large dashes). Subband energies are indicated by horizontal lines. Note in (a) that the second subband remains populated in the field range shown, apart from a temporary depopulation around 8.2 T.

In our model we keep the electron density fixed and assume a Gaussian broadened DOS with a width that increases with the square root of the magnetic field [7]. As the (bare) spin splitting is too small to have an effect, it is neglected in the calculations. The Landau-level broadening is our only fit parameter and the calculated oscillation amplitude increases with decreasing broadening. However, even in the limit of nonbroadened Landau levels, the calculated amplitude of the oscillations saturates to only  $0.7\mu_B^*$  per electron.

Using the self-consistent model, we have calculated the Fermi energy as a function of magnetic field, from which the magnetization follows directly through the Maxwell proportionality. The dashed line in Figure 5.1 shows the resulting magnetization for a Gaussian Landau-level broadening with

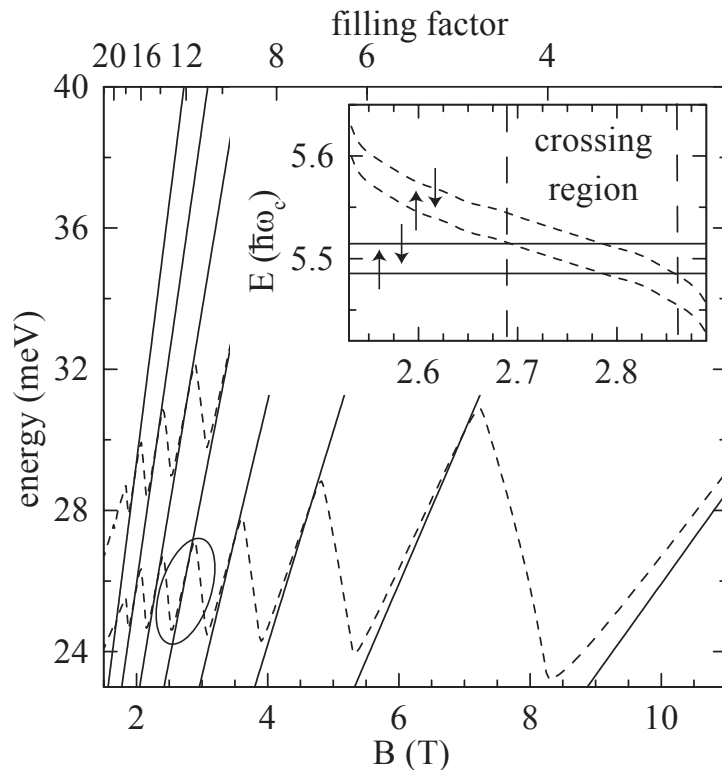


Figure 5.3: Landau-level diagram of the dual-subband 2DEG. Solid lines depict levels originating from the lower subband. Dashed lines show the Landau-levels of the higher subband. The inset is an enlargement of the circled Landau-level crossing around  $\nu = 11.9$ ; energy-levels are normalized to the cyclotron energy.

$\Gamma = 0.2\sqrt{B}$  meV. It is in very good agreement with the experimental data as it reproduces all three observed effects: triangular shape, non- $1/B$ -periodicity, and the reduced amplitude.

Inspection of the self-consistent field-dependent modeling of the high-density 2DEG in detail reveals two important points. First, although the number of electrons in the highest subband is small, it remains populated up to high magnetic fields. This can be clearly seen in Figure 5.2(a), which plots the populations of both subbands resulting from our self-consistent calculations. Second, the shape of the Fermi energy (and thus

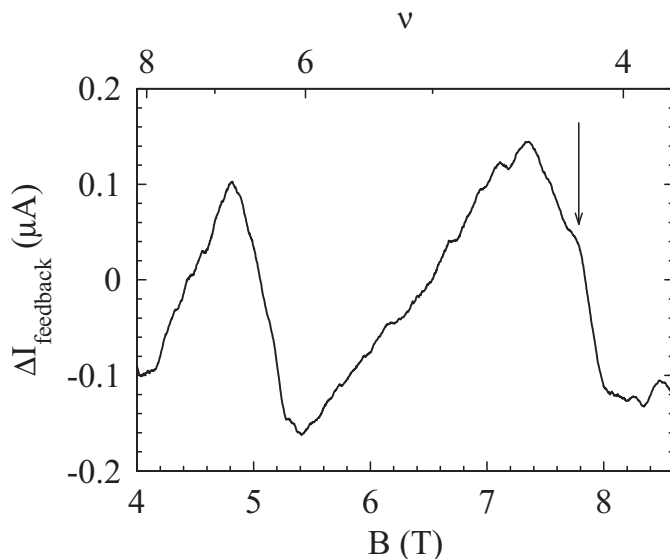


Figure 5.4: Magnetometry data at 1.5 K: a kink (down arrow) is clearly visible near  $B = 7.8$  T, when the second subband temporarily depopulates. While the downward slope before the kink is mainly determined by the redistribution of electrons over the subbands, the small, finite width of the sharp step following the kink is determined by a background DOS.

magnetization) is almost completely determined by the oscillations in the intersubband spacing, caused by self-consistent redistribution of electrons over the two subbands. The effect of this redistribution is illustrated in Fig. 5.2(b), which shows three distinctly different confining potentials with their respective subband energies at three values of the magnetic field. A Landau-level scheme for the dual-subband 2DEG, resulting from the self-consistent model, is depicted in Figure 5.3.

While levels originating in the lower subband (solid lines) are linear functions of the magnetic field, the Landau levels of the higher subband (dashed lines) oscillate according to the intersubband spacing. Above 1.5 T only the lowest Landau level of the second subband is populated and the Fermi energy is pinned to this level.

It is interesting to remark that consequently the width of the magnetization step is mainly caused by this redistribution and not by a finite DOS

between two Landau levels as shown for a single subband 2DEG [14, 18] (chapter 4.2.1). Only in the region near  $\nu = 4$  there is, scarcely visible in Figure 5.1, a kink followed by a sharp step. This feature is more pronounced when we look at a blow-up of the data in this region. Figure 5.4 shows a single measurement of the feedback-current (after subtraction of a smooth background) as a function of magnetic field at 1.5 K. At the field where the second subband depopulates, indicated by the arrow in fig. 5.4, the decreasing magnetization changes to a sharp step, whose finite width is related to this small, extra DOS. Similar kinks are not visible on the other downward slopes, where the width is determined by the electron redistribution. It is possible to include the extra DOS in the self-consistent model, but this does not influence the shape of the calculated Fermi energy.

## 5.4 Exchange-enhanced ground states

At 1 K, additional minima appear in the 2DEG's magnetization (Fig. 5.5) around filling factor  $\nu = 9.6$ ,  $\nu = 12.0$ , and  $\nu = 14.2$ , indicated by down arrows in fig. 5.5. These filling factors correspond to positions where two Landau levels originating from the two subbands cross.

On the flanks of the triangular oscillations a series of crossings occurs between the lowest Landau level of the higher subband and Landau levels with decreasing index of the lower subband as the magnetic field increases (see figure 5.3). A close-up of one of the level crossings, when we include the spin-splitting, is shown in the inset of fig. 5.3. When spin is included, there is a small region where the levels with different spin consecutively cross each other. In this region spin up and spin down do not alternate with increasing energy: the two spin-up levels are lowest in energy, the spin-down levels the highest.

The Landau levels in Figure 5.3 are in reality broadened, creating an overlap and giving the electrons some freedom to distribute themselves over the available energy levels. We suggest that therefore electrons may form a novel electronic ground state that is spin polarized in the crossing region. Creation of this polarized state would be favored by the system, because exchange interaction significantly reduces the ground-state energy. When the energy gain exceeds the broadening of the energy levels,

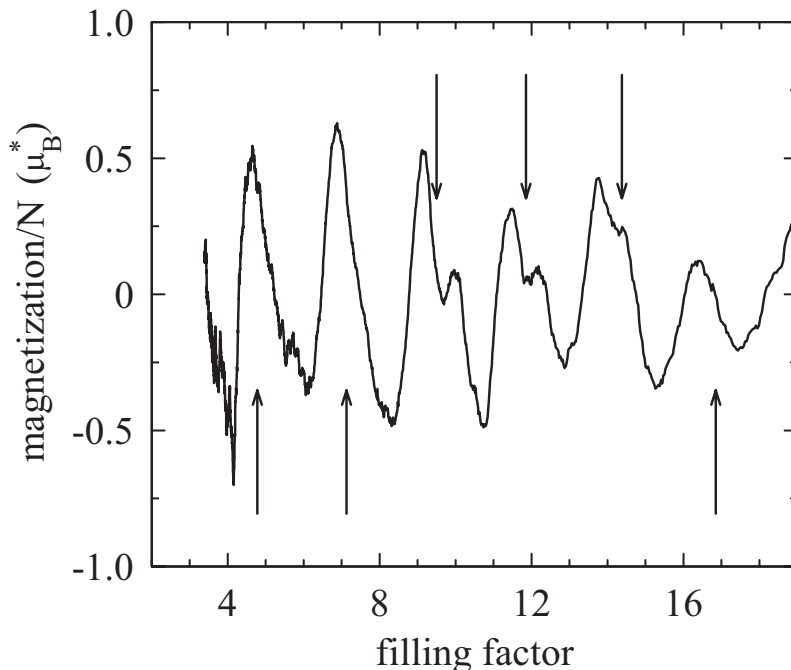


Figure 5.5: Magnetization of a dual-subband 2DEG at 1 K. Arrows indicate the positions of Landau-level crossings, additional features can be seen at these positions in intermediate magnetic fields.

the enhanced gap shows up as a minimum in the magnetization.

Although it is evident that at lower magnetic fields (filling factors higher than 14, up arrows indicate the positions of the level crossings) extra structure cannot be seen due to the width of the Landau levels, extra structure is also too small to be observed at the Landau-level crossings of the lowest filling factors (up arrows in Fig. 5.5). A possible explanation is the reduction of the effective number of electrons participating in the crossing from two in the four crossing levels to one or less, making it impossible to gain energy via exchange. Clearly the picture of the crossing region sketched above is not yet complete and further experimental and theoretical investigation of this many-body effect is required.



## 5.5 Conclusion

In summary, we have measured the magnetization of coupled 2DEGs in a dual-subband 2DEG in a GaAs/AlGaAs heterojunction. We find that the de Haas-van Alphen oscillations are changed in three ways compared to those of the single 2DEG. The shape is triangular, the oscillation amplitude is reduced to  $0.5\mu_B^*$  and the oscillations are no longer periodic in  $1/B$ . This behavior is well described by a self-consistent model, taking into account changes of the confining potential with magnetic field. It shows the shape of the Fermi energy and consequently the magnetization is entirely dominated by the oscillations in this potential due to redistribution of electrons over the two subbands. We observe additional magnetization minima at 1 K, which occur at magnetic fields corresponding to the positions where Landau levels originating in the two different subbands cross. These minima possibly originate from a reduction of the total energy by the formation of a novel, exchange enhanced electronic state at the level crossing.

## 5.6 Acknowledgments

We would like to thank M. Elliot for fruitful discussion.

## References

- [1] S. Das Sarma and A. Pinczuk, *Perspectives in Quantum Hall Effects* (Wiley, New York, 1997).
- [2] V. Piazza, V. Pellegrini, F. Beltram, W. Wegscheider, T. S. Jungwirth, and A. H. MacDonald, *Nature* **402**, 638 (1999).
- [3] E. P. De Poortere, E. Tutuc, J. Papadakis, and M. Shayegan, *Science* **290**, 1546 (2000).
- [4] J. Jaroszyński, T. Andrearczyk, G. Karczewski, J. Wróbel, T. Wojtowicz, E. Papis, E. Kamińska, A. Piotrowska, D. Popović, and T. Dietl, *Phys. Rev. Lett.* **89**, 266802 (2002).

- 
- [5] W. Pan, H. L. Stormer, D. C. Tsui, L. N. Pfeiffer, K. W. Baldwin, and K. W. West, Phys. Rev. B **64**, 121305 (2001).
- [6] K. Muraki, T. Saku, and Y. Hirayama, Phys. Rev. Lett. **87**, 196801 (2001).
- [7] T. Ando, A. B. Fowler, and F. Stern, Rev. Mod. Phys. **54**, 437 (1982).
- [8] F. Stern and S. Das Sarma, Phys. Rev. B **30**, 840 (1984).
- [9] A. S. Alexandrov and A. M. Bratkovsky, Phys. Rev. B **63**, 033105 (2001).
- [10] A. S. Alexandrov and A. M. Bratkovsky, Phys. Rev. Lett. **76**, 1308 (1996).
- [11] R. A. Shepherd, M. Elliott, W. G. Herrenden-Harker, M. Zervos, P. R. Morris, M. Beck, and M. Ilegems, Phys. Rev. B **60**, R11277 (1999).
- [12] D. Shoenberg, *Magnetic oscillations in metals, Cambridge monographs on physics* (Cambridge University Press, Cambridge, 1984).
- [13] J. P. Eisenstein, H. L. Störmer, V. Narayanamurti, and A. C. Gossard, Superlattice Microstruct. **1**, 11 (1985).
- [14] S. A. J. Wieggers, M. Specht, L. P. Lévy, M. Y. Simmons, D. A. Ritchie, A. Cavanna, B. Etienne, G. Martinez, and P. Wyder, Phys. Rev. Lett. **79**, 3238 (1997).
- [15] M. R. Schaapman, P. C. M. Christianen, J. C. Maan, D. Reuter, and A. D. Wieck, Appl. Phys. Lett. **81**, 1041 (2002).
- [16] J. Sanchez-Dehesa, F. Meseguer, F. Borondo, and J. C. Maan, Phys. Rev. B **36**, 5070 (1987).
- [17] S. Trott, G. Paasch, G. Gobsch, and M. Trott, Phys. Rev. B **39**, 10232 (1989).
- [18] M. P. Schwarz, M. A. Wilde, S. Groth, D. Grundler, C. Heyn, and D. Heitmann, Phys. Rev. B **65**, 245315 (2002).

*Magnetization of a two-dimensional electron gas with a second filled subband*

---

## Chapter 6

# Magnetization of bilayer two-dimensional electron systems

### Abstract

We present a torque-magnetometry study of two bilayer two-dimensional electron gases with different inter-layer barrier widths of 25 Å and 40 Å. At filling factors where a symmetric-anti-symmetric (SAS) transition occurs, we clearly observe steps in magnetization, even though this transition is purely electronic in nature and no direct change of spin or orbital angular momentum is involved. The size and occurrence of these SAS magnetization steps are explained quantitatively through thermodynamics. In addition the apparent size of the magnetization steps at Landau-level transitions is significantly reduced compared to a single layer two-dimensional electron system. This reduction cannot be accounted for by a subtraction of the SAS energy-gap, and we speculate it could be due to an in-plane component of the magnetization.

---

Part of this work has been published in:

M. R. Schaapman, U. Zeitler, P. C. M. Christianen, J. C. Maan, D. Reuter, and A. D. Wieck, Phys. E **22**, 86 (2004).

## 6.1 Introduction

In the past decade, the study of the bilayer two-dimensional electron gas (2DEG) has led to the discovery of new electronic ground states and other interesting phenomena (see [1] and references therein). Amongst the more spectacular of these are the observed absence of integer quantum Hall states [2–4], the formation of even denominator fractional quantum Hall states [5–7], and the discovery of quantum Hall ferromagnetism at energy-level crossings [8]. One of the features that makes the bilayer system particularly interesting is the additional, single, controllable degree of freedom associated with the third dimension.

For the strongly coupled bilayer the electron wavefunctions form symmetric and anti-symmetric combinations that are split in energy by an energy gap  $\Delta$ SAS. This additional energy gap also influences the Landau levels of the 2DEG, as already described in chapter 2.2.2. As a consequence the chemical potential shows additional steps,  $\Delta$ SAS in size, when the Landau-levels from the anti-symmetric state depopulate in an increasing magnetic field. In a (macroscopic) thermodynamic picture, the Maxwell relation between chemical potential  $\mu$  and magnetization  $M$  states that such a  $\Delta$ SAS step should be measured as a magnetization step with a size of  $N_{total}/B \times \Delta$ SAS, with  $N_{total}$  the total number of electrons in the bilayer 2DEG and  $B$  the magnetic field. On the other hand, thermodynamics is a macroscopic approach and it does not give a microscopic description of the system. Microscopically, the  $\Delta$ SAS energy gap is determined by the shape of the confining potential, and none of the quantum numbers normally associated with magnetism, such as orbital angular momentum and spin, change. This raises the question if we will indeed observe a change in magnetization of the bilayer 2DEG at  $\Delta$ SAS transitions.

In this chapter we present a magnetization study of such bilayer 2DEGs. To investigate the effect of inter-layer coupling (for which the size of  $\Delta$ SAS is a measure), we use two bilayer systems with different inter-layer barriers and electron densities. As activated transport measurements will show,  $\Delta$ SAS is reduced by an in-plane magnetic field. The magnetization of the bilayer 2DEG with the highest  $\Delta$ SAS is therefore also determined at a second, higher tilt angle.

We will show that a change in magnetization does occur at the symmetric-anti-symmetric transition. The occurrence and sizes of the

magnetization steps at  $\Delta$ SAS are explained in terms of thermodynamics. Additional to the symmetric-anti-symmetric steps, we also observe different behavior compared to that of the single 2DEG in Chapter 4 at the Landau-level transitions: in the bilayer 2DEGs the oscillation amplitude is significantly reduced. This reduction cannot be accounted for by subtraction of  $\Delta$ SAS and is tentatively ascribed to an additional in-plane magnetic moment

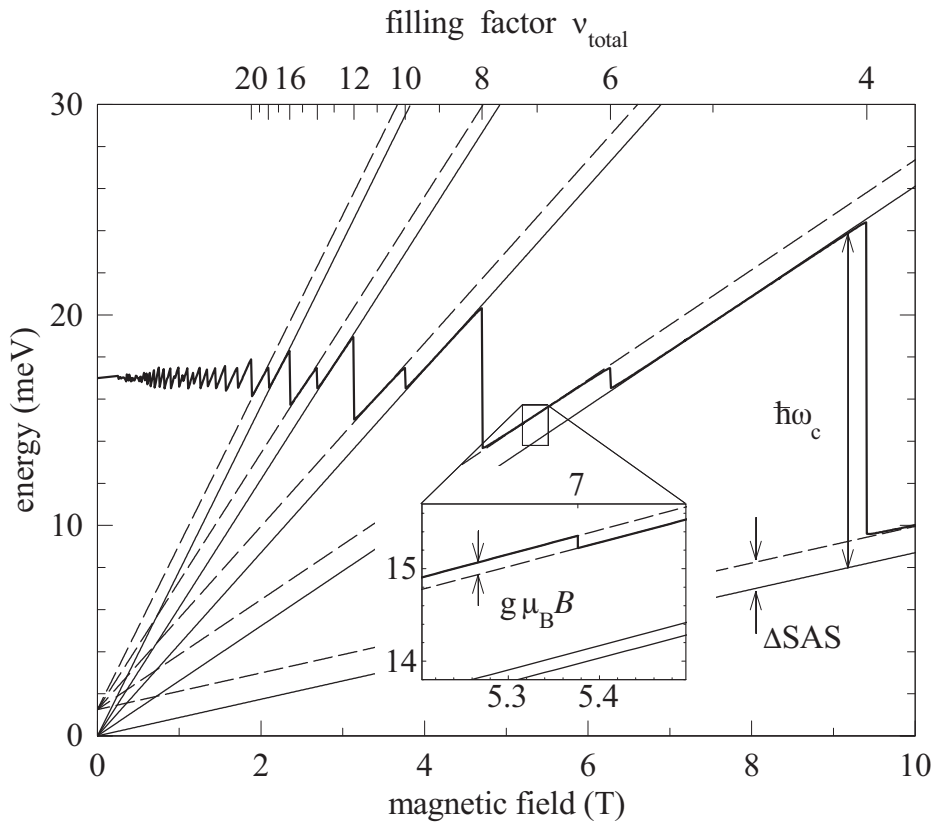


Figure 6.1: Energy level scheme in a bilayer 2DEG with  $n = 9.1 \cdot 10^{11} \text{ cm}^{-2}$  and a barrier of  $40 \text{ \AA}$ . The two Landau level fans of the symmetric (thin solid line) and anti-symmetric energy levels (thin dashed line) are clearly visible. The Fermi energy (thick solid line) oscillates as a function of magnetic field: Landau, SAS and spin transitions occur at  $\nu_{\text{total}} = 4n$  ( $n$  is a positive integer),  $4n - 2$ , and odd  $n$  respectively.

## 6.2 Experimental results

Using the sensitive torque-magnetometry technique discussed in chapter 3 [9], we study the magnetization of two bilayer 2DEGs, formed in symmetric double quantum wells. As was already noted in chapter 2.2.2, in a magnetic field both the symmetric and the anti-symmetric energy level in this confining potential split into a fan of Landau-levels, and each level is again split into two by spin-splitting. This is illustrated in Figure 6.1 that shows an energy-level diagram representative of our samples. Landau-levels originating in the symmetric energy-level are indicated by thin solid lines, Landau-levels of the anti-symmetric energy-level by the thin dashed lines. The samples are chosen to have a  $\Delta$ SAS larger than the spin gap ( $g\mu_B B$ ), which is enlarged in the inset as it is not resolved on the larger scale. However,  $\Delta$ SAS is still small compared to the Landau-level splitting ( $\hbar\omega_c$ ) in the magnetic range of the experiment. The Fermi-energy is shown as a thick solid line, it oscillates as a function of magnetic field and can be clearly seen to jump across the  $\Delta$ SAS gap.

Both our samples are MBE grown GaAs/AlGaAs double quantum wells with an AlGaAs inter-well barrier. The fraction of Al in the barrier is 0.34. Sample 1 has a total electron density of  $n_{\text{total}} = 9.1 \cdot 10^{11} \text{ cm}^{-2}$ , well widths of 104 Å, and a barrier thickness of 40 Å. Self-consistent calculations suggest a size of 1.25 meV for  $\Delta$ SAS. Sample 2 has a lower total electron density of  $n_{\text{total}} = 7.5 \cdot 10^{11} \text{ cm}^{-2}$ , 101 Å wells, and a 25 Å barrier. The thinner barrier results in a larger  $\Delta$ SAS, which is calculated to be 1.56 meV. Both bilayer 2DEGs are balanced, tunnel-coupled systems. Additional to the contact-free samples used for the magnetometry, we also use a Hall-bar processed from the same wafer as sample 2. This Hall-bar allows us to determine the dependence of  $\Delta$ SAS on the tilt angle between the 2DEG and the magnetic field from transport measurements.

### 6.2.1 Magnetization of the 40 Å barrier bilayer 2DEG

As a first example, Figure 6.2 shows the magnetization, defined as the magnetic moment of the feedback coil<sup>1</sup>, of the bilayer with the 40 Å barrier

---

<sup>1</sup>For a single 2DEG with a magnetization strictly perpendicular to the 2DEG plane, this is precisely equal to the magnetic moment of the 2D electron gas.

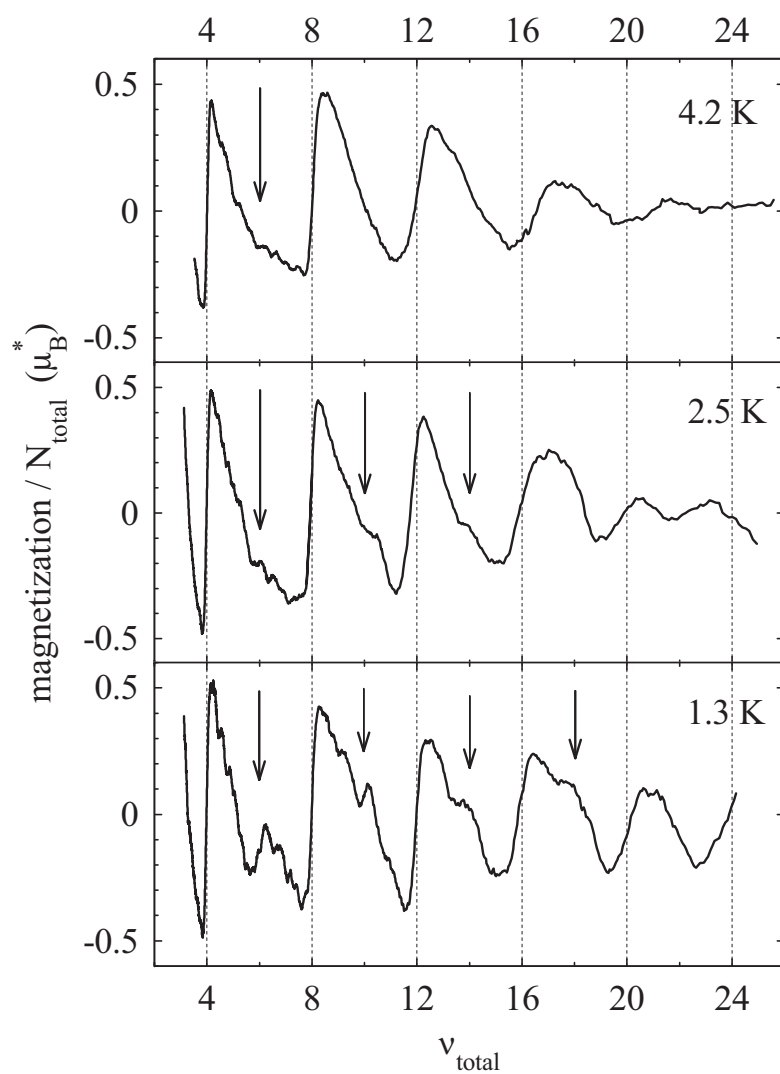


Figure 6.2: Magnetization of the bilayer 2DEG with a 40 Å barrier at 4.2 K (top), 2.5 K (middle), and 1.3 K (bottom). Oscillations are periodic in  $\nu_{\text{total}}$ . The large steps at  $\nu_{\text{total}} = 4n$  (with  $n$  a positive integer) are related to Landau-levels splitting. Features related to  $\Delta$ SAS ( $\nu_{\text{total}} = 4n - 2$ ) are indicated by arrows.



(sample 1) as a function of total filling factor  $\nu_{\text{total}} = hn_{\text{total}}/eB_{\perp}$ . The magnetization is normalized to the total number of electrons in the bilayer 2DEG, and it is shown for three different temperatures: 4.2 K (top), 2.5 K (middle), and 1.3 K (bottom).

The magnetization at 4.2 K (Fig. 6.2, top) shows the large, periodic Landau-level transition steps at  $\nu_{\text{total}} = 4n$  (with  $n$  a positive integer). The amplitude of these Landau steps in the magnetization is discussed in section 6.4. In between them we see a developing shoulder in the magnetization where a  $\Delta$ SAS transition takes place at  $\nu_{\text{total}} = 6$ , indicated by an arrow in Fig. 6.2, top. When the temperature is lowered to 2.5 K, more shoulders can be seen (Fig. 6.2, middle), and their number continues to increase as the temperature is lowered to 1.3 K. At the lowest total filling factors of  $\nu_{\text{total}} = 6$  and 10 (highest magnetic fields) shoulders have developed into minima (Fig. 6.2, bottom), providing the first experimental evidence that the electronic  $\Delta$ SAS transition indeed gives a step in the magnetization as predicted by thermodynamics.

## 6.3 The symmetric-anti-symmetric energy-splitting $\Delta$ SAS

### 6.3.1 Tilt-angle dependence of $\Delta$ SAS

As we have seen, the presence of the additional SAS energy-splitting changes the magnetization of the bilayer 2DEG. To investigate the  $\Delta$ SAS steps, we measure the magnetization of sample 2 (25 Å barrier) at two tilt angles: the standard 12° and the larger 23°. An increase in tilt angle corresponds to an increase in in-plane magnetic field, which is known to influence  $\Delta$ SAS [1–3]. To improve our understanding of the effect of an in-plane magnetic field on the magnetization, we first determine the tilt-angle dependence of  $\Delta$ SAS separately by means of a transport experiment.

We use a Hall-bar processed from the same wafer as sample 2 to find the energy gap at  $\nu_{\text{total}} = 6, 10,$  and 14 from thermally activated transport. This technique determines the energy gap from the temperature dependence of minima in the longitudinal resistance  $R_{xx}$  of the bilayer 2DEG. The resistance of each minimum in  $R_{xx}$  depends exponentially on the inverse of the temperature; the value of the exponent is equal to the size

of the corresponding energy gap reduced by the energy-level broadening. This means a series of measurements similar to the one used to determine the effect of the laser in chapter 3.2.3, shown in Fig. 3.4(b), is done for each  $\nu_{\text{total}}$  of interest. To study the dependence of  $\Delta$ SAS on tilt angle, measurements are repeated at various tilt angles.

The range of angles,  $0^\circ$ – $45^\circ$ , is chosen such that the values of the activation energies at  $\nu_{\text{total}}=6, 10,$  and  $14$  are determined by  $\Delta$ SAS. At these angles  $\hbar\omega_c$  is larger than  $\Delta$ SAS, which in turn is larger than the spin splitting that determines the activation energies at odd  $\nu_{\text{total}}$ . At larger angles, starting from about  $50^\circ$ , the characters of the energy gaps change [1–3]. For these high angles the spin splitting  $g\mu_B B$  (determined by the total magnetic field) exceeds  $\Delta$ SAS (reduced by an in-plane magnetic field, see below). As a consequence the energy gaps at filling factors  $\nu_{\text{total}}=6, 10,$  and  $14$  are now determined by  $g\mu_B B$  and  $\Delta$ SAS gaps occur

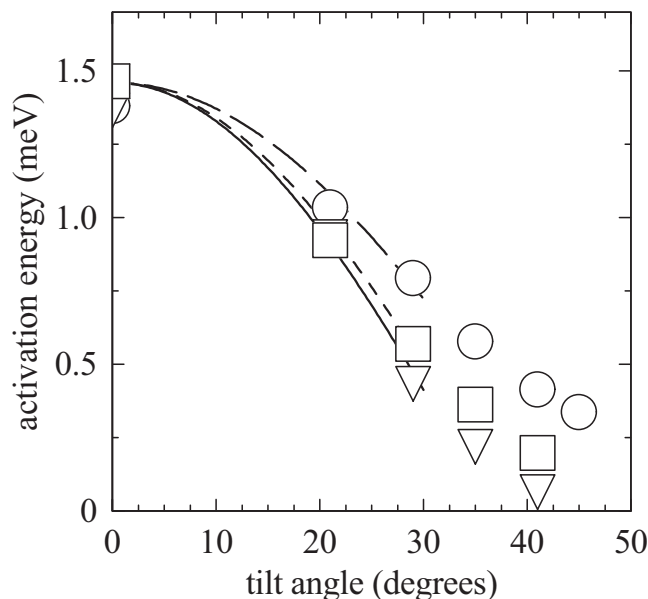


Figure 6.3: Tilt angle dependence of the energy gap at  $\nu_{\text{total}}=6$  (○), 10 (□), and 14 (▽) in the bilayer 2DEG with a 25 Å barrier. The gap is determined from thermally activated transport measurements, lines are added to guide the eye.

at odd filling factors.

Figure 6.3 shows the tilt angle dependence of the  $\Delta$ SAS activation energy for  $\nu_{\text{total}}=6$  ( $\circ$ ), 10 ( $\square$ ), and 14 ( $\nabla$ ). In perpendicular magnetic field we find a value for the activation gap of 1.46 meV for all filling factors, in reasonable agreement with the self-consistently calculated and field-independent value for  $\Delta$ SAS of 1.56 meV.  $\Delta$ SAS decreases with increasing tilt angle, or increasing in-plane magnetic field as expected [1–3].

### 6.3.2 Effect of $\Delta$ SAS on the magnetization

Returning to the effect of the additional SAS-splitting on the magnetization of the bilayer 2DEG, Figure 6.4 shows this magnetization for three different types of inter-layer coupling (size of  $\Delta$ SAS). Fig. 6.4(a) again shows (for comparison) the magnetization of sample 1 with the 40 Å inter-layer barrier, mounted at the standard tilt angle of 12°. Fig. 6.4(b) presents the magnetization of sample 2 with the 25 Å inter-layer barrier, mounted at the same tilt angle of 12°. Finally, Fig. 6.4(c) plots the magnetization for the same bilayer, sample 2, but now mounted at the higher tilt angle of 23°. In the Figure magnetization steps originating from Landau-level transitions are indicated by LL, steps due to the SAS-splitting are indicated by  $\Delta$ SAS. All measurements shown in Fig. 6.4 are taken at the lowest experimental temperatures. At these temperatures the LL steps have all reached their saturation sizes. For sample 1 only the  $\Delta$ SAS step at  $\nu_{\text{total}}=6$  has reached its maximum size. For sample 2, at both tilt angles, not only the step at  $\nu_{\text{total}}=6$ , but all the SAS steps are fully developed.

We will first consider more closely the magnetization of sample 2 at the tilt angle of 12°, plotted in Fig. 6.4(b). In the magnetization, steps arising from the transitions across all three different types of energy gaps in the bilayer 2DEG (Landau-level,  $\Delta$ SAS, and spin, illustrated in Fig. 6.1), including the spin gap that was not observed in sample 1, can now be seen. Spin splitting, indicated by S-arrows, is visible as shoulders at  $\nu_{\text{total}}=5, 6$ , and 7. This observation indicates a sizeable enhancement of the spin gap as its bare value is below our detection limit, as we have also seen for the single-layer 2DEG in chapter 4. Steps at the electronic  $\Delta$ SAS transitions can clearly be seen at  $\nu_{\text{total}}=6, 10$ , and 14. In this 25 Å barrier sample the inter-layer coupling is larger resulting in a larger  $\Delta$ SAS than in the 40 Å barrier sample, and as therefore expected, the corresponding

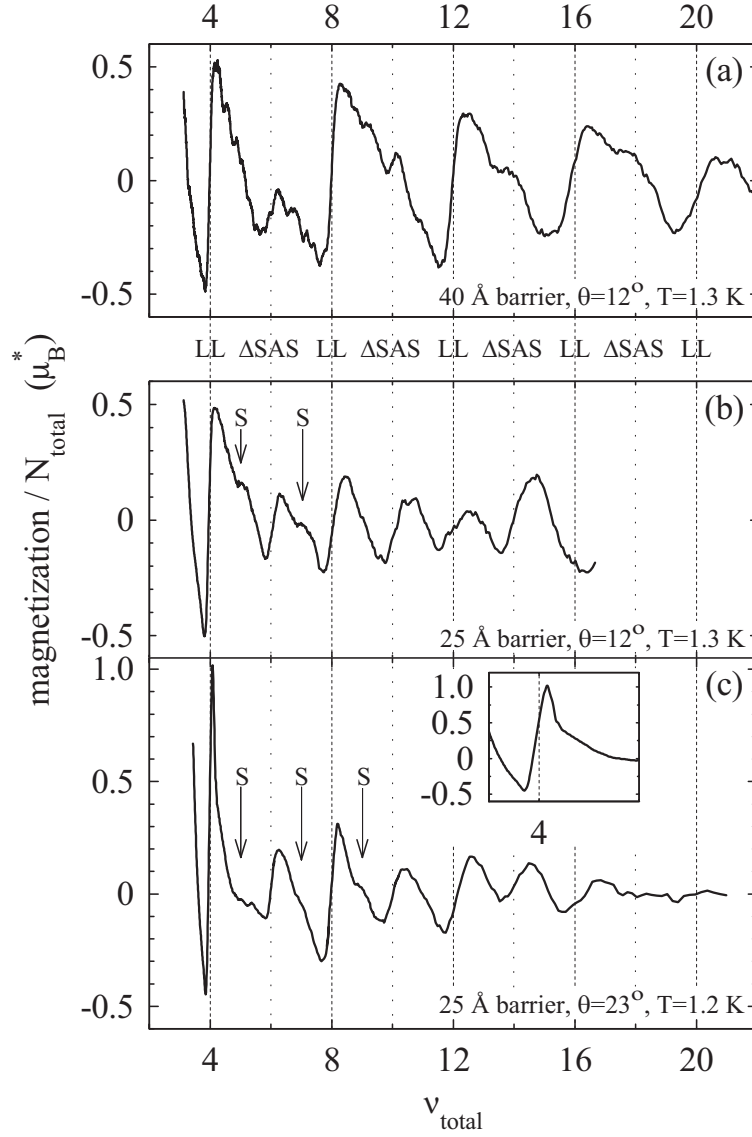


Figure 6.4: Magnetization of sample 1 with an inter-layer barrier of 40 Å, mounted at a tilt angle of  $12^\circ$  (a), and sample 2 with a barrier of 25 Å, mounted at  $12^\circ$  (b) and  $23^\circ$  (c). Inset (c) shows the additional feature at  $\nu_{\text{total}}=4$ , further discussed in 6.4.1. Spin transitions are indicated by arrows with S, Landau-level transitions by LL. Note the difference in  $\Delta$ SAS between (a), (b) and (c).

steps are significantly larger for sample 2 (Fig. 6.4(b)) than for sample 1 (Fig. 6.4(a)).

In sample 2 we see that while at the lower filling factors  $\Delta$ SAS is indeed smaller than the measured Landau-level steps, at the highest filling factors (lowest magnetic fields), the  $\Delta$ SAS step ( $\nu_{\text{total}}=14$ ), actually becomes larger. This is easily understood since Landau gaps increase linearly with the magnetic field, while  $\Delta$ SAS is determined by the inter-layer barrier, and is therefore approximately independent of the field. As a result  $\Delta$ SAS magnetization steps are dominant at low magnetic fields. The value of  $\Delta$ SAS in this sample, calculated to be 1.56 meV, is large enough for the corresponding magnetization steps to become comparable to and even larger than the Landau-level steps at lower magnetic fields (higher filling factors).

Next, we increase the tilt angle of sample 2 with respect to the magnetic field from  $12^\circ$  to  $23^\circ$ . The magnetization<sup>2</sup> at this larger tilt angle is shown in Figure 6.4(c); again steps arising from transitions across all three different types of energy gaps can be seen. Although spin-splitting is still the smallest,  $\Delta$ SAS the medium and Landau-level splitting the largest energy gap, their relative sizes have changed due to the higher tilt angle. First, as evidenced by Fig. 6.3, the larger in-plane field resulting from the higher tilt angle affects the coupling between the two layers of electrons, reducing  $\Delta$ SAS [1]. This behavior is reflected in the magnetization: a comparison of Figures 6.4(b) and (c) shows that with increasing tilt angle the  $\Delta$ SAS magnetization steps, clearly visible at  $\nu_{\text{total}}=6, 10, \text{ and } 14$ , have indeed become smaller, as expected.

Second, because the Zeeman-splitting is dependent on the *total* magnetic field while the position of the magnetization steps (and the size of the Landau gap) is dependent on the *perpendicular* magnetic field, the spin gap increases relative to the (reduced)  $\Delta$ SAS and the Landau gap. When we qualitatively compare the magnetization at the tilt angle of  $12^\circ$  (Fig. 6.4(b)) to that at the tilt angle of  $23^\circ$  (Fig. 6.4(c)), we indeed see the relative size of the spin-splitting has increased; the shoulder at  $\nu_{\text{total}}=5$  has become much larger, and an additional spin-related shoulder is observed

---

<sup>2</sup>To obtain this higher angle, the sample is mounted at an additional angle of  $11^\circ$  with respect to the feedback coil, which remains at  $12^\circ$ . The magnetization is now defined as the component of the magnetic moment of the feedback coil normal to the bilayer 2DEG.

at  $\nu_{\text{total}}$  of 9.

### 6.3.3 Size of the $\Delta$ SAS energy-splitting

The observation of a change in the magnetic moment at a symmetric-anti-symmetric transition that is electronic in nature and does not involve either spin or orbital angular momentum at first sight seems surprising, but it can be understood in terms of thermodynamics. The Maxwell equation that relates magnetization and chemical potential is reduced to a proportionality for a 2DEG (Chapter 2.3.3). Thus any change in the chemical potential, such as  $\Delta$ SAS (spin is neglected), will give a proportional change in the magnetization. This also means that via this Maxwell proportionality the value of the  $\Delta$ SAS energy-splitting can be calculated directly from the size of the magnetization step at the SAS transition:

$$\frac{\Delta M}{\Delta \mu} = \frac{N}{B} \quad (6.1)$$

$$\Delta \text{SAS} = \frac{\Delta M}{N} B \quad (6.2)$$

When the 2DEG is tilted with respect to the magnetic field, only the perpendicular component should be used for  $B$ .

In the magnetization measured at the lowest experimental temperature, shown in Figure 6.4, the  $\Delta$ SAS step in the highest experimental magnetic field, corresponding to  $\nu_{\text{total}} = 6$ , has reached its maximum saturation value for sample 1 as well as sample 2. We can therefore quantify and compare  $\Delta$ SAS for both samples and tilt angles at this filling factor.

For sample 1 with the 40 Å inter-layer barrier the magnetization step at  $\nu_{\text{total}} = 6$  is 0.8 meV in size at 1.3 K. Taking into account Landau level broadening, this is in reasonable agreement with the value of 1.25 meV obtained from a self-consistent calculation for  $\Delta$ SAS. For sample 2 with the 25 Å inter-layer barrier, mounted at the same tilt angle of 12°, we deduce the size of  $\Delta$ SAS from this magnetization step to be 1.5 meV. This value is significantly larger than the 0.8 meV found for sample 1, as expected due to the thinner barrier. Again the experimentally found value corresponds well to the value suggested by self-consistent calculation of 1.56 meV. It also corresponds well to the activation gap deduced from transport measurements (Fig. 6.3) of 1.3 meV. When the tilt angle of

sample 2 is increased to  $23^\circ$ , the step size at  $\nu_{\text{total}}=6$  is reduced to a value of 1.4 meV. The reduction of  $\Delta\text{SAS}$  with increasing in-plane magnetic field is in qualitative agreement with the tilt angle dependence of the  $\Delta\text{SAS}$  activation gap.

As we have seen in Figures 6.4(b) and 6.4(c), for sample 2 the magnetization steps at  $\nu_{\text{total}}=10$  and 14 have also reached their maximum values, i.e. they no longer increase with decreasing temperature, allowing a comparison between values of  $\Delta\text{SAS}$  determined at different magnetic fields. Figures 6.4(b) and 6.4(c) show that, although the sizes of the magnetization steps  $\Delta M$  are smaller for the higher tilt angle,  $\Delta M$  is more or less constant as a function  $\nu_{\text{total}}$  for each tilt angle. Because a higher  $\nu_{\text{total}}$  corresponds to a lower magnetic field, when Equation 6.2 is then used to calculate  $\Delta\text{SAS}$ , a constant  $\Delta M$  suggests a strongly  $\nu_{\text{total}}$ -dependent  $\Delta\text{SAS}$  (values are collected in Table 6.1). This is not in agreement with the picture that  $\Delta\text{SAS}$ , determined by the confining potential, is magnetic field independent, nor is it consistent with the values found from activated transport measurements. Figure 6.3 shows that at a tilt angle of  $12^\circ$  the activation gap has a filling factor independent value of 1.3 meV. When the tilt angle is increased to  $23^\circ$  the values for  $\nu_{\text{total}}=6, 10$  and 14 diverge slightly to 1.0 meV, 0.87 meV and 0.82 meV, but this difference is still not very significant compared to the values extracted from magnetization measurements (1.4 meV, 0.60 meV, and 0.35 meV; Table 6.1).

To understand the apparent discrepancy between the values for  $\Delta\text{SAS}$  determined from magnetization and those determined from activated transport, it is important to realize that in Equation 6.2 the change in chemical potential  $\Delta\mu = \Delta M/N \times B$  is strictly speaking only equal to  $\Delta\text{SAS}$  when the density of states (DOS) is a series of  $\delta$ -functions. When, for example, the width in magnetic field of a magnetization step between two energy-levels is large enough for the values of these levels to change significantly during the step (both increase linearly with magnetic field), this is not a good approximation and Equation 6.2 will underestimate  $\Delta\text{SAS}$ . We will therefore first look more closely at the precise shape of the magnetization steps.

In the bilayer 2DEG, as we have seen for the single layer 2DEG in chapter 4.2.1 and in one specific instance in the dual-subband 2DEG shown in fig. 5.4, the steps in the magnetization are not infinitely sharp. All steps, both at Landau-level and at  $\Delta\text{SAS}$  transitions, have a finite width. In

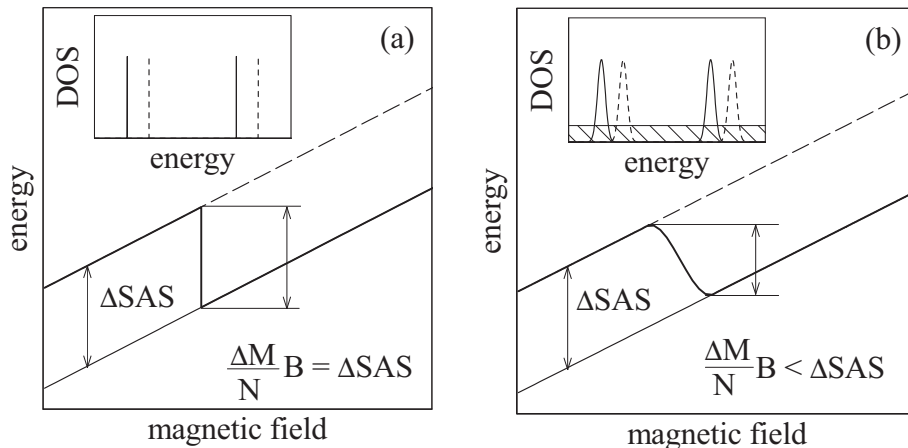


Figure 6.5: Effect of the shape of the DOS (insets) on the transition from the anti-symmetric energy-level (dashed line) to the symmetric energy-level (thin solid line). For the ideal system with a DOS of  $\delta$ -functions the magnetization step is proportional to  $\Delta SAS$  (a). With a DOS of broadened peaks and a background (hatched area) the magnetization step is reduced, making the energy gap seem smaller than  $\Delta SAS$  (b).

chapter 4.2.1 this width was associated with the presence of a background density of states, and the fraction of states in the gap was calculated using the approach by Wiegers et al. [10]. This approach is now also employed to find the fraction of states in the bilayer gaps, using the data presented in Fig. 6.4.

For sample 1 we find an average, constant fraction of states in the gap of 6%. We find a fraction of 7% when sample 2 is mounted at a tilt angle of  $12^\circ$  and a smaller fraction of 6% when it is mounted at the larger angle of  $23^\circ$ . For both bilayer 2DEGs, in contrast to the single layer 2DEG, the fraction of states in the gap is constant, i.e. not a function of  $\nu_{\text{total}}$ , in all gaps, irrespective of their size. The observed constancy of this fraction supports the supposition that the non-zero DOS in the gap is really due to a background DOS, and not an overlapping of tails of Gaussian broadened DOS peaks.

We now return to the apparent filling-factor dependence of the  $\Delta SAS$  calculated from magnetization steps using Equation 6.2 for sample 2. With



Table 6.1: Size of the changes in chemical potential in sample 2 determined from the measured  $\Delta M$  and calculated taking finite step widths into account.

tilt angle	$\nu_{\text{total}}$	measured	calculated
		$\Delta M/N \times B$ (meV)	$\Delta\mu$ (meV)
12°	6	1.5	1.4
	10	0.85	0.84
	14	0.66	0.63
23°	6	1.4	1.1
	10	0.62	0.60
	14	0.3	0.35

an ideal DOS of  $\delta$ -functions, the step in magnetization is infinitely sharp and  $\Delta M/N \times B$  is equal to  $\Delta\text{SAS}$ , illustrated in Fig. 6.5(a). However, as we have seen, in reality the shape of the DOS is more complex: it consists of a combination of broadened peaks with a constant background, schematically shown in the inset of Fig. 6.5(b), resulting in a finite width of the steps in the magnetization. For the relatively small  $\Delta\text{SAS}$  energy-splitting the finite width of the step cannot be neglected: the step maximum occurs at a significantly lower magnetic field and the step minimum at a significantly higher magnetic field than the single field value associated with  $\nu_{\text{total}}$ . Because Landau-levels are linear functions of the magnetic field, the gap  $\Delta M/N \times B$  observed in magnetization is therefore smaller than  $\Delta\text{SAS}$  as illustrated in Figure 6.5(b). We can see from Fig. 6.5 that while  $\Delta\text{SAS}$  remains the same,  $\Delta M/N \times B$  will become smaller for transitions at higher filling factors, because there the Landau levels are steeper. This reduction will be stronger for smaller  $\Delta\text{SAS}$ .

To determine whether the  $\nu_{\text{total}}$ -dependence of the energy gaps calculated from the magnetization steps can be explained fully by the finite step width or whether  $\Delta\text{SAS}$  is  $\nu_{\text{total}}$ -dependent, we calculate the change in chemical potential with this finite step width effect taken into account but using a fixed value for  $\Delta\text{SAS}$  (1.56 meV for the tilt angle of 12° and

1.40 meV for the tilt angle of  $23^\circ$ ). Table 6.1 shows that the  $\Delta\mu$  found from this calculation is in good agreement with the energy gap  $\Delta M/N \times B$ . This therefore leads to the conclusion that also in magnetization measurements  $\Delta$ SAS can be considered independent of filling factor, or magnetic field, in accordance with the behavior of the activation gap determined from transport measurements.

In summary the observed change in the magnetic moment at a SAS-transition, corresponding to a change in magnetization, can be explained through thermodynamics. At  $\nu_{\text{total}}=6$ , where finite step width effects are small enough to be neglected, the size of the magnetization step corresponds to the expected (calculated) size of  $\Delta$ SAS, as well as to the activation energy determined from activated transport measurements for both samples and tilt angles. It is interesting to note that although this result is thermodynamically correct, it gives no information on the microscopic origin of the involved change in magnetic moment by a purely electronic transition, which remains intriguing.

## 6.4 Reduced oscillations at Landau gaps

### 6.4.1 Magnetization at Landau-level transitions

Next to the observation of a change in the magnetization of the bilayer 2DEG at the electronic SAS transition, the magnetization steps at the Landau-level transitions are also different compared to those in a single-layer 2DEG (chapter 4). If we look more closely at the Landau-level steps in Figure 6.2, we see that, interestingly, the amplitude of the magnetization oscillations at Landau-level transitions is much smaller than  $1 \mu_B^*$  per electron.

To investigate if the reduction is a temperature effect, and find the final size of the magnetization amplitudes at the steps, we determine the temperature dependence of these oscillation amplitudes. Figure 6.6 plots the magnetization amplitude at the Landau-level steps at  $\nu_{\text{total}} = 4$  ( $\circ$ ), 8 ( $\square$ ), 12 ( $\triangle$ ), 16 ( $\nabla$ ), and 20 ( $\boxtimes$ ) for sample 1 with the 40 Å inter-layer barrier. While the value at the two highest filling factors initially still increases approximately exponentially in size with  $1/T$ , amplitudes all saturate to a constant value at 1.3 K. This value is only  $0.49 \mu_B^*$  per electron at  $\nu_{\text{total}} = 4$ , much less than the  $1 \mu_B^*$  per electron we have seen in

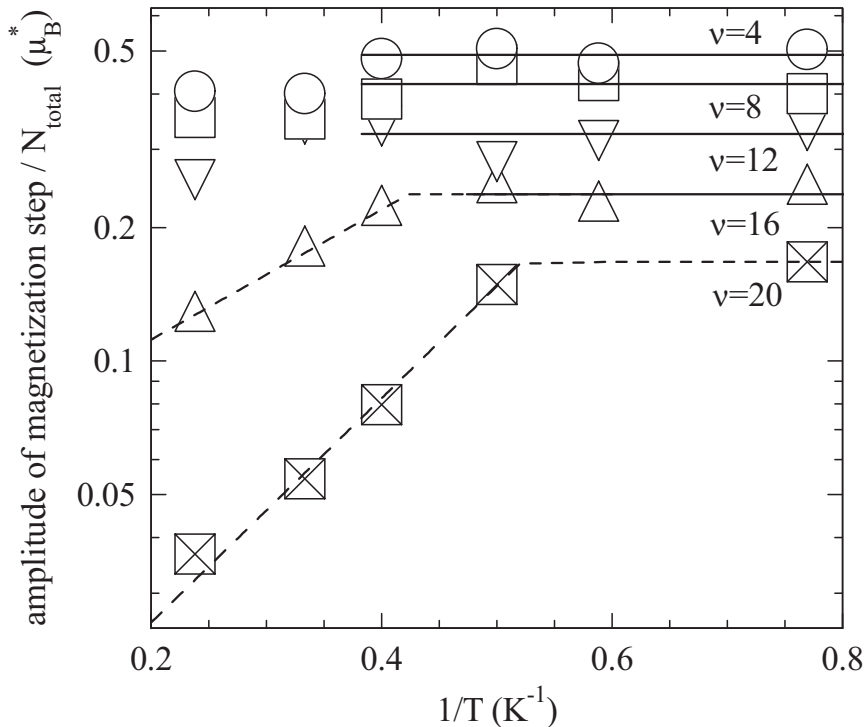


Figure 6.6: Amplitude of the magnetization oscillations at the Landau-level transitions  $\nu_{total} = 4$  (○), 8 (□), 12 (△), 16 (▽), and 20 (⊠) in sample 1 (40 Å barrier) as a function of temperature. The steps at  $\nu_{total}=16$  and 20 increase exponentially with  $1/T$  (dashed lines are added to guide the eye), and all step-sizes saturate at values considerable lower than  $1 \mu_B^*$  per electron (solid lines).

chapters 2.3.2 and 4, and decreases with increasing filling factor. As the oscillation amplitude of the magnetization no longer grows with decreasing temperatures, we conclude the observed reduction is not a temperature effect. The magnetization steps at Landau-level transitions in sample 2 show a similar reduction at both tilt angles in Figures 6.4(b) and (c).

For the higher tilt angle of  $23^\circ$ , at  $\nu_{total}=4$  (the Landau-level transition in the highest magnetic field), surprisingly, prominently visible, and contrary to the measurements at the lower tilt angle of  $12^\circ$ , a sharp feature develops on top of the saw-tooth. This feature increases with decreasing

temperature and reaches an amplitude of  $1 \mu_B^*$  per electron at 1.2 K (inset of Fig. 6.4(c)). The shape and size of the peak do not depend on the sweep rate or sweep direction of the magnetic field, and we therefore rule out the non-equilibrium Eddy current discussed in chapter 2.3.1 as an explanation. At present the physical nature of this additional feature is unclear and requires further study. In the following analysis of the de Haas-van Alphen oscillations we will therefore only consider the actual saw-tooth and leave this peak out of our considerations.

A comparison of all measurements in Fig. 6.4 shows that, interestingly, the magnetization oscillation amplitude at  $\nu_{\text{total}}=4$  is  $0.5 \mu_B^*$  in all three cases, while  $\Delta\text{SAS}$  is different for each one. However, the size of the Landau-level steps in the magnetization decreases much more rapidly with increasing filling factor for sample 2 than for sample 1. The decrease is strongest at the smaller tilt angle of  $12^\circ$ , where  $\nu_{\text{total}}=16$  is, in fact, absent altogether.

### 6.4.2 In-plane magnetization

In a bilayer the Landau-level transition is a transition from the symmetric energy-level in the higher Landau-level to the anti-symmetric energy-level in the Landau-level below it (see Fig.6.1) and the measured energy gap  $\hbar\omega_c$  is therefore reduced by  $\Delta\text{SAS}$ . In principle  $\hbar\omega_c$  ( $1.7 \text{ meV/T} \times B$ ) is also reduced by spin-splitting. However,  $g\mu_B B$  ( $25 \mu\text{eV/T} \times B$ ) is two orders of magnitude smaller, and although  $g$  can be enhanced by exchange interaction (4.2.2), at Landau-level transitions the numbers of electrons with spin up and spin down are equal, making the enhancement minimal. The effect of spin-splitting can therefore safely be ignored. The reduction of  $\hbar\omega_c$  by  $\Delta\text{SAS}$  is a relatively small effect and can by no means account for the observed large reduction. Because a reduction of the cyclotron energy  $\hbar\omega_c$  is not a likely explanation for the observed step-size reduction, it is important to consider what quantity is really measured in our experiment.

The magnetization measured by our torsional magnetometry technique (chapter 3) is the magnetic moment generated in the feedback-coil, mounted to the 2DEG, to keep the tilt angle  $\theta$  of the sample fixed. In other words we measure the torque  $\Gamma$  generated by the magnetic moment of the 2DEG and  $\Gamma/B$  is only equal to the measured magnetization if this moment is perpendicular to the 2DEG. When the magnetic moment of

the sample makes a deviation angle  $\phi$  away from the normal due to the presence of an in-plane component to the magnetization  $M_{\parallel}$ , the torque is reduced to

$$\Gamma = MB \sin(\theta - \phi) \quad (6.3)$$

and the measured magnetization that assumes  $\phi = 0$  is smaller than the actual magnetization of the 2DEG<sup>3</sup>.

The bilayer 2DEG has an extra degree of freedom in the third dimension, introduced by the addition of the second quantum well. A conceivable consequence of this is a dependence of the free energy  $F$  of the bilayer on the in-plane magnetic field  $B_{\parallel}$ , and then its partial derivative  $-\partial F/\partial B_{\parallel} = M_{\parallel}$  would be non-zero. We tentatively suggest this is the case and that therefore the reduction of the measured magnetization is not due to a reduction of the size of the total, real, magnetization (proportional to the energy gap), but rather due to a reduction of torque by a small magnetization component parallel to the magnetic field in the plane of the bilayer 2DEG.

When the sample is mounted at the standard tilt angle of  $12^\circ$ , the in-plane magnetization component is nearly perpendicular to the magnetic field, and as a result it exerts a large counter torque even when its size is small. Unfortunately Eq. 6.3 has two unknown variables for our single, experimental value of the reduction, but the size of  $M_{\parallel}$  can be estimated if it is assumed to be additional, i.e. the perpendicular magnetization component is assumed to be  $1 \mu_B^*$  per electron in amplitude. We estimate that if only 10% of the total magnetization is associated to the parallel component, this would be sufficient to effectuate a collapse in the measured magnetization by a factor of two, i.e. the value we observe at  $\nu_{\text{total}}=4$ .

### 6.4.3 Filling factor dependence of the reduction

Figure 6.7 shows the filling-factor dependence of the magnetization oscillation amplitude for sample 1, with the  $40 \text{ \AA}$  inter-layer barrier, mounted at a tilt angle of  $12^\circ$  ( $\circ$ ), and sample 2, with the  $25 \text{ \AA}$  inter-layer barrier mounted at the tilt angle of  $12^\circ$  ( $\square$ ) as well as a larger tilt angle of  $23^\circ$

---

<sup>3</sup>We conform to the commonly used definition used by Shoenberg [11](chapter 2.3.2), where this is equal to the magnetic moment.

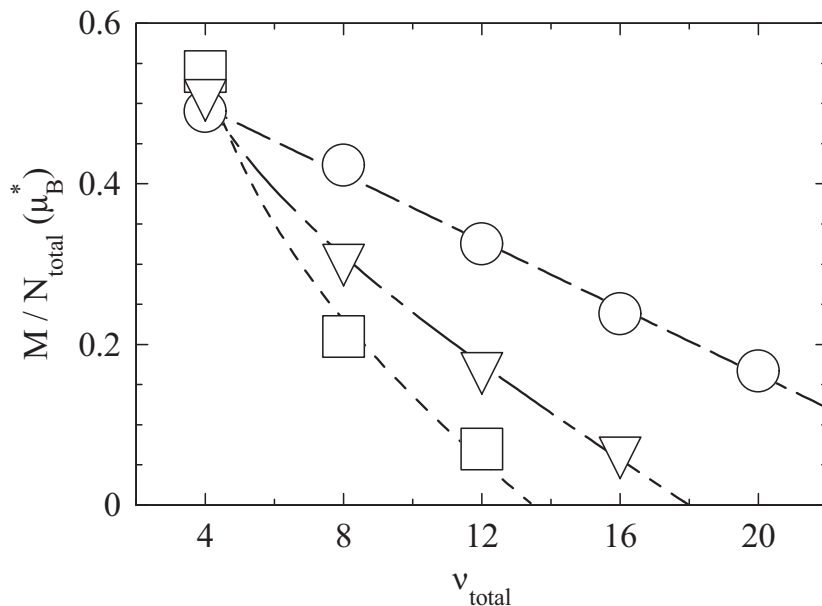


Figure 6.7: Filling-factor dependence of the magnetization amplitude of the Landau-level steps for sample 1, with the 40 Å barrier, mounted at a tilt angle of 12° (○), and for sample 2, with the 25 Å barrier, mounted at tilt angles of 12° (□), and 23° (▽). Note that all amplitudes are much smaller than 1  $\mu_B^*$  per electron. The long dashed line is a linear fit for sample 1, the small dashed and dash-dotted lines for sample 2 have an additional  $1/\nu_{\text{total}}$  component.

(▽). The collapse of the observed magnetization amplitude from 1 to 0.5  $\mu_B^*$  per electron can be clearly seen at  $\nu_{\text{total}}=4$ .

Although the filling-factor dependence of the magnetization amplitude of sample 1 can be described as linear, an extra component is needed to describe sample 2. The  $\nu_{\text{total}}$  dependence given by the, at this stage, phenomenological relation

$$\Delta M = a + b \cdot \nu_{\text{total}} + \frac{c}{\nu_{\text{total}}} \quad (6.4)$$

is in good agreement with our data. In this equation  $\Delta M$  is the total magnetization step, equal to twice the amplitude plotted in Fig. 6.7. To

interpret the information obtained by fitting Eq. (6.4) to the data, we use the Maxwell proportionality Eq. (6.1) to translate this equation into

$$\Delta\mu = \alpha B + \beta + \gamma B^2 \quad (6.5)$$

Here it is important to realize that strictly this is only correct if the magnetization is perpendicular to the 2DEG, and the total size of the energy gap will be underestimated when this is not the case.

We can now assign the components that make up the filling-factor dependence. The first component is an energy gap that increases linearly with magnetic field, a property characteristic for Landau-level gaps. As  $\alpha$  will only reflect the total energy gap when the magnetization is strictly perpendicular to the 2DEG, and as we suspect this is not the case, we only use the parameter  $a$  as a fitting parameter. The second component of Equation (6.5) is a magnetic-field independent energy gap. In all cases  $\beta$  has a negative value, it therefore represents a constant gap by which the Landau-level splitting is reduced. From Figure 6.1  $\beta$  can easily be identified as  $\Delta\text{SAS}$ .

The Landau-level steps in sample 1 are entirely determined by these two components that make up the linear function plotted by the large dashed line in Fig. 6.7. The value of  $\beta$  determined from the slope is 1.35 meV, this  $\Delta\text{SAS}$  value is in good agreement with the 1.25 meV resulting from self-consistent calculations. It is interesting to see that also here the magnetization of the bilayer 2DEG is influenced by the purely electronic SAS transition. Figure 6.7 clearly shows the magnetization amplitude does not reach  $1 \mu_{\text{B}}^*$  per electron when extrapolated to  $\nu_{\text{total}}=0$ , but only  $\alpha = 0.6 \mu_{\text{B}}^*$  per electron. In other words, the reduction of the step size cannot be accounted for by  $\Delta\text{SAS}$ . Because the decrease is linear, we can conclude that the reduction to  $0.6 \mu_{\text{B}}^*$  per electron of the oscillation amplitude at Landau-level steps (after compensating for  $\Delta\text{SAS}$ ) due to  $M_{\parallel}$ , does not vary with  $\nu_{\text{total}}$ . The assumption of an amplitude of  $M_{\perp} = 1 \mu_{\text{B}}^*$  per electron then suggests a fixed deviation angle, as defined in 6.4.2, of  $\phi = 5^{\circ}$ .

The addition of the third,  $1/\nu_{\text{total}}$  component to Equation (6.4) provides a good description of the Landau-level steps in sample 2. To understand this we will first look at the value of the parameter  $c$ . While still using the parameter  $a$  as a fitting parameter, we now fix  $b$  at the known values of  $\Delta\text{SAS}$  of 1.5 meV and 1.4 meV, expressed in the appropriate

units. We find that for the tilt angle  $\theta = 12^\circ$   $c$  is  $3.1 \mu_B^*$  per electron, and for the tilt angle  $\theta = 23^\circ$   $c$  equals  $1.5 \mu_B^*$  per electron. The product  $c^* = c \sin(\theta)$  is the same for both tilt angles, suggesting the last component of Eq. (6.4) can be described as a contribution proportional to the in-plane magnetic field with a proportionality that is a constant for the bilayer.

Because the parallel component of the magnetic field plays a role, the translation of  $c$  into  $\gamma$  is not straightforward and it can only be said that the sign of both is the same, namely positive. Two interpretations of this contribution present themselves: it can represent either an energy gap reduced by a value proportional to  $B^2$ , or a torque that is directly proportional to  $B$ . Although it is well-known that a parallel magnetic field can reduce the Landau-level splitting, this effect is negligible for our samples. Moreover, such a reduction *increases* with increasing in-plane field, which is not in agreement with Figure 6.7, pointing to the  $B$ -proportional torque as a more likely explanation. The field-dependence of the reduction of  $\Gamma$  points in the direction of a field-dependent deviation angle  $\phi$  that decreases with increasing  $B$ .

Figure 6.7 shows that the amplitude reduction is strongest for the largest  $\Delta$ SAS. It also suggests that the field-dependence of the deviation is largest for the largest  $\Delta$ SAS and absent for the smallest  $\Delta$ SAS. This indicates the effect increases with increasing inter-layer coupling.

## 6.5 Conclusion

We have investigated the effect of inter-layer coupling on the magnetization of 2D electron systems by measuring the magnetization of two bilayer 2DEGs with different inter-layer barriers at two tilt angles in the magnetic field.

We clearly observe a step in the magnetization at filling factors corresponding to  $\Delta$ SAS transitions, although this transition is electronic in nature and does not involve a change in spin or orbital angular momentum. This observation is quantitatively explained in terms of thermodynamics. For both samples the step sizes are in agreement with the values suggested by self-consistent calculations where  $\Delta$ SAS does not depend on the magnetic field.



In addition the apparent size of the oscillations at Landau-level transitions is significantly smaller than  $1 \mu_B^*$  per electron. We speculate this could be due to an in-plane magnetization component. As a consequence the magnetization is no longer strictly normal to the bilayer 2DEG, resulting in a smaller measured torque.

## References

- [1] S. Das Sarma and A. Pinczuk, *Perspectives in Quantum Hall Effects* (Wiley, New York, 1997).
- [2] G. S. Boebinger, H. W. Jiang, L. N. Pfeiffer, and K. W. West, Phys. Rev. Lett. **64**, 1793 (1990).
- [3] Y. W. Suen, J. Jo, M. B. Santos, L. W. Engel, S. W. Hwang, and M. Shayegan, Phys. Rev. B **44**, 5947 (1991).
- [4] A. H. MacDonald, P. M. Platzman, and G. S. Boebinger, Phys. Rev. Lett. **65**, 775 (1990).
- [5] H. A. Fertig, Phys. Rev. B **40**, 1087 (1989).
- [6] J. P. Eisenstein, G. S. Boebinger, L. N. Pfeiffer, K. W. West, and S. He, Phys. Rev. Lett. **68**, 1383 (1992).
- [7] Y. W. Suen, L. W. Engel, M. B. Santos, M. Shayegan, and D. C. Tsui, Phys. Rev. Lett. **68**, 1379 (1992).
- [8] V. Piazza, V. Pellegrini, F. Beltram, W. Wegscheider, T. S. Jungwirth, and A. H. MacDonald, Nature **402**, 638 (1999).
- [9] M. R. Schaapman, P. C. M. Christianen, J. C. Maan, D. Reuter, and A. D. Wieck, Appl. Phys. Lett. **81**, 1041 (2002).
- [10] S. A. J. Wieggers, M. Specht, L. P. Lévy, M. Y. Simmons, D. A. Ritchie, A. Cavanna, B. Etienne, G. Martinez, and P. Wyder, Phys. Rev. Lett. **79**, 3238 (1997).
- [11] D. Shoenberg, *Magnetic oscillations in metals, Cambridge monographs on physics* (Cambridge University Press, Cambridge, 1984).

# Summary

This thesis describes a study of the magnetization of electrons confined to two dimensions. First the two-dimensional electron gas (2DEG) that is formed in structures made of the semiconducting materials GaAs and AlGaAs is introduced in chapter 2 together with the 2DEG's magnetic properties. After this the purposely developed torsional magnetometry technique is presented in chapter 3. This technique is then employed to experimentally investigate the magnetization of 2DEGs made up of one component (chapter 4) as well as that of 2DEGs made up of more, interacting components (chapters 5 and 6). Key questions in these investigations are 1) what determines the shape and size of the magnetization and 2) how it is affected by the interaction between different components.

In order to detect the small magnetization of a 2DEG, a sensitive magnetometer is required. Chapter 3 describes the developed torque magnetometer with optical angular detection in detail and characterizes its most important components: the quadrant detector, the influence of the laser, and the feedback system. The quadrant detector is used to measure the rotation of the sample. It outputs a normalized, laser intensity independent position signal and can detect rotations as small as  $10^{-7}$  rad. The effect of the laser light on the sample is determined from in-situ 2DEG transport measurements. At laser intensities below 2 mW no adverse effects on the sample are found. By using a feedback system the magnetization is directly determined quantitatively. It has the additional advantage of actively damping the mechanical vibrations that limit the sensitivity.

The magnetometer has a sensitivity of  $10^{-12}$  J/T when operated in a Bitter-magnet and  $2 \times 10^{-13}$  J/T at 15 T in a superconducting magnet. To demonstrate the sensitivity and versatility, chapter 3 presents magnetization measurements of the organic conductor  $\kappa$ -(BEDT-TTF)<sub>2</sub>Cu(NCS)<sub>2</sub> as well as of a multiband 2DEG.

Chapter 4 experimentally investigates the single 2DEG, described by a simple, analytical model (in chapter 2). The main features of the measured magnetization are well described by the analytical model: they form a sharp,  $1/B$ -periodic sawtooth with an amplitude of  $1\mu_B^*$  per electron. Contrary to the calculated saw-tooth, however, the steps in the magnetization have a small, but finite width attributed to a background density of states. At 1.2 K additional shoulders corresponding to spin transitions are visible, suggesting a spin-gap enhanced by many-body interactions.

The density of electrons in the 2DEG can be increased far enough for a second electronic subband in the heterojunction to be occupied. Such a dual-subband 2DEG is the subject of investigation in chapter 5. In contrast to the single subband 2DEG, the magnetization now shows non- $1/B$ -periodic, triangularly shaped oscillations with a significantly smaller amplitude of about  $0.5 \mu_B^*$  per electron. A field-dependent self-consistent model quantitatively explains all three effects. The model shows the confining potential in the heterojunction changes significantly when a magnetic field is applied and demonstrates that the shape of the magnetization is dominated by oscillations in this potential. Additionally, at the lowest temperature of 1 K, small oscillations become visible at magnetic fields where Landau levels of the two subbands cross.

Finally, chapter 6 presents the magnetization of a second type of multi-component 2DEG: the bilayer 2DEG realized in a double quantum well. This system has an extra energy gap ( $\Delta$ SAS) that is determined by the barrier separating the wells. The magnetization of two bilayer 2DEGs with barriers of 40 Å and 25 Å is investigated. Although the nature of  $\Delta$ SAS is purely electronic, a step in the magnetization is clearly observed at the magnetic field where this transition takes place. The occurrence and size of the step are quantitatively explained in terms of thermodynamics; the values of  $\Delta$ SAS given by the magnetization steps are in good agreement with calculated values. Surprisingly, the apparent size of the amplitude of the magnetization oscillations associated with the Landau-level transitions is significantly less than the typical  $1\mu_B^*$  per electron. This reduction cannot be accounted for by simply subtracting  $\Delta$ SAS, and it suggests the magnetization has an in-plane component. The dependence of the reduction on sample and magnetic field indicates that the resulting deviation angle of the magnetization increases with increasing inter-layer coupling.

# Samenvatting

Dit proefschrift beschrijft een studie naar de magnetisatie van elektronen waarvan de bewegingsvrijheid beperkt is tot twee richtingen. Hoofdstuk 2 introduceert dit twee-dimensionale elektronen gas (2DEG), gevormd in structuren gemaakt van de halfgeleiders GaAs en AlGaAs, samen met zijn magnetische eigenschappen. Hierna beschrijft hoofdstuk 3 de speciaal ontwikkelde torsie magnetometrie techniek. Deze techniek wordt vervolgens gebruikt om experimenteel onderzoek te doen naar de magnetisatie van 2DEGs met één (hoofdstuk 4) of meer, gekoppelde componenten (hoofdstukken 5 en 6). De sleutelvragen hierbij zijn: 1) Wat bepaalt de vorm en grootte van de magnetisatie? en 2) Hoe wordt dit beïnvloed door de interactie tussen de componenten?

Om de kleine magnetisatie van een 2DEG te kunnen detecteren, is een gevoelige magnetometer nodig. In hoofdstuk 3 wordt de ontwikkelde torsie magnetometer met optische hoek uitlezing in detail beschreven en worden de belangrijkste onderdelen gekarakteriseerd: de kwadrant detector, de invloed van de laser en het feedback-systeem. Met de kwadrant detector wordt de rotatie van het sample gemeten. De detector geeft een genormaliseerde positie coördinaat, die onafhankelijk is van de laser intensiteit. Op deze manier kunnen hoeken tot  $10^{-7}$  rad opgelost worden. De invloed van de laser op het sample wordt bepaald uit in-situ transport metingen. Bij intensiteiten onder 2 mW zijn er geen ongewenste effecten. Door gebruik te maken van een feedback-systeem kan de magnetisatie direct, kwantitatief bepaald worden. Een bijkomend voordeel is de actieve demping van de mechanische trillingen die de gevoeligheid beperken.

De magnetometer heeft een gevoeligheid van  $10^{-12}$  J/T bij gebruik in een Bitter-magneet en van  $2 \times 10^{-13}$  J/T bij 15 T in een supergeleidende magneet. Om de gevoeligheid en veelzijdigheid te demonstreren, laat hoofdstuk 3 magnetisatie metingen zien van zowel de organische geleider

$\kappa$ -(BEDT-TTF)<sub>2</sub>Cu(NCS)<sub>2</sub> als een multi-subband 2DEG.

In hoofdstuk 5 wordt een enkel 2DEG, zoals beschreven door een simpel, analytisch model in hoofdstuk 2, experimenteel onderzocht. De vorm van de gemeten magnetisatie wordt in hoofdlijnen goed beschreven door het model: het is een scherpe,  $1/B$ -periodieke zaagtand met een amplitude van  $1\mu_B^*$  per elektron. Echter, in tegenstelling tot het model hebben de stappen in de magnetisatie een kleine, maar eindige breedte, die wordt toegeschreven aan een achtergronds toestandsdichtheid. Bij 1.2 K zijn extra schouders te zien die overeen komen met spin-overgangen, wat suggereert dat de spin-splitsing wordt vergroot door veel-deeltjes wisselwerking.

De dichtheid van elektronen in het 2DEG kan ver genoeg verhoogd worden om een tweede elektronische subband in de heterojunctie te bezetten. Een dergelijk twee-band systeem vormt het onderwerp van hoofdstuk 5. In tegenstelling tot bij het 2DEG met een enkele band, laat de magnetisatie nu niet- $1/B$ -periodieke, driehoekige oscillaties zien met een gereduceerde amplitude van ongeveer  $0.5 \mu_B^*$  per elektron. Een veldafhankelijk, zelf-consistent model verklaart deze drie effecten kwantitatief. Het model laat zien dat de opsluitpotentiaal in de heterojunctie significant verandert in een magnetisch veld en het demonstreert dat de vorm van de magnetisatie wordt bepaald door oscillaties in deze potentiaal. Hiernaast worden bij de laagste temperatuur van 1 K kleine oscillaties zichtbaar bij magnetische velden waar Landau niveaus van de twee subbanden elkaar kruisen.

Tot slot wordt in hoofdstuk 6 de magnetisatie van een tweede type multi-component 2DEG gepresenteerd: het dubbellaags 2DEG in een dubbele kwantum put. Dit systeem heeft een extra energie splitsing ( $\Delta$ SAS) die wordt bepaald door de barrière tussen de putten. Twee dubbellen met barrières van  $40 \text{ \AA}$  en  $25 \text{ \AA}$  worden onderzocht. Hoewel  $\Delta$ SAS puur elektronisch van aard is, zijn er toch duidelijke stappen in de magnetisatie zichtbaar bij magnetische velden waar deze overgang optreedt. Het optreden en de grootte van de stappen worden kwantitatief verklaard door de thermodynamica. De waarden van  $\Delta$ SAS bepaald uit magnetisatie komen goed overeen met berekende waarden. Verrassend genoeg is de amplitude van de magnetisatie oscillaties bij Landau overgangen een stuk kleiner dan de typische  $1\mu_B^*$  per electron. Dit suggereert dat de magnetisatie een component heeft in het 2D vlak. De manier waarop de reductie afhangt van sample en magneet veld impliceert dat de resulterende deviatie hoek van de magnetisatie toeneemt met toenemende koppeling tussen de lagen.

# List of publications

*Magnetization of multi-component two-dimensional quantum-Hall systems.*

M.R. Schaapman, U. Zeitler, P.C.M. Christianen, J.C. Maan, D. Reuter, and A.D. Wieck, *Physica E* **22**, 86 (2004).

*Magnetization of a two-dimensional electron gas with a second filled subband.*

M.R. Schaapman, U. Zeitler, P.C.M. Christianen, J.C. Maan, D. Reuter, A.D. Wieck, D. Schuh, and M. Bichler, *Physical Review B* **68**, 193308 (2003).

*Magnetization of a double-layer and of a double-subband two-dimensional electron gas.*

M.R. Schaapman, U. Zeitler, P.C.M. Christianen, J.C. Maan, D. Reuter, and A.D. Wieck, in: A.K. Long and J.H. Davies, editors, *The Physics of Semiconductors 2002*.

*A multipurpose torsional magnetometer with optical detection.*

M.R. Schaapman, P.C.M. Christianen, J.C. Maan, D. Reuter, and A.D. Wieck, *Applied Physics Letters* **81**, 1041 (2002).

*Dipole-dipole coupling in Mn<sub>12</sub>-acetate.*

J.A.A.J. Perenboom, M.R. Schaapman, S.O. Hill, J.S. Brooks, and N.S. Dalal, in: Z. Fisk, L. Gor'kov, and R. Schrieffer, editors, *Physical Phenomena at High Magnetic Fields*, World Scientific, Singapore, 469 (1998).

*List of publications*

---

# Curriculum Vitae

Maaïke Ruth Schaapman was born on the 25<sup>th</sup> of June, 1975 in Delft. After attending the American Embassy School in New Delhi, India from 1987 to 1989, she attended the grammar school "Stedelijk Gymnasium" in Nijmegen, where she graduated in June 1994.

She studied physics at the University of Nijmegen from 1994 to 1999. The last year of these studies she worked on a graduation project at the High Field Magnet Laboratory in the experimental solid state physics group of Prof. dr. ir. J. C. Maan, resulting in the masters thesis entitled "Magnetization studies of Mn<sub>12</sub>-acetate".

Starting in 1999 she was consecutively employed as a PhD-student at the High Field Magnet Laboratory of the University of Nijmegen. She spent her time developing a new magnetometry technique and applied it to investigate properties of various low-dimensional electron systems. The results of this work are contained in this thesis.